MORPHOLOGICAL AND FUNCTIONAL CONSEQUENCES OF THE LAND-TO-WATER TRANSITION IN THE SALAMANDER FAMILIES AMBYSTOMATIDAE AND PLETHODONTIDAE

BY

HANNAH ELIZABETH DARCY

DISSERTATION

Submitted in partial fulfillment of the requirements
for the degree of Doctor of Philosophy in Biology
with a concentration in Ecology, Ethology and Evolution
in the Graduate College of the
University of Illinois Urbana-Champaign, 2023

Urbana, Illinois

Doctoral Committee:

Associate Professor Philip S.L. Anderson, Chair and Director of Research
Assistant Professor Sandy Kawano, The George Washington University
Associate Professor Charles Roseman
Professor Andrew Suarez

ABSTRACT

Land-to-water transitions are major evolutionary events and introduce new constraints to tetrapod morphology. Two North American salamander groups have recolonized aquatic habitats: mole salamanders (Ambystomatidae) and lungless salamanders (Spelerpini; Plethodontidae). I examined the morphological and biomechanical consequences of this transition using a comparative approach. First, I tested the hypothesis that aquatic species have convergent skull morphologies, given the different developmental pathways followed by the two groups. Using 3D microCT scan data from online repositories and museum specimens, I performed a geometric morphometric analysis on skull shape and applied a phylomorphospace to the morphometric data to determine whether morphological variation was due to phylogeny or ecology. Second, I performed nanoindentation tests on cartilage and bone from dissected Ambystoma to determine if Young's modulus differed significantly between aquatic and terrestrial taxa, and to determine the difference in magnitude between cartilage and bone. Finally, to focus more closely on a structure primarily involved in feeding, I examined the mandibular morphology and functional performance in the two families. I tested the importance of morphology and Young's modulus values in the mandible in resisting forces that simulated prey-capture by holding shape volume and applied loads constant in a Finite Element Model. While there are statistically significant differences in the jaw proportions in aquatic and terrestrial salamanders in both families, the mechanical models did not support that terrestrial morphologies are better suited for applying bite forces. The results of these four studies will guide future work investigating the functional demands on salamander skulls and what structural changes occur when terrestrial species recolonize aquatic habitats.

ACKNOWLEDGMENTS

First, I would like to thank my doctoral advisor, Dr. Phil Anderson, for taking a chance on me in his first cohort of PhD students as the stubborn salamander person in a fish lab. I'm grateful for all of the support and feedback over the years from current and former members of the Anderson lab: Dr. Stephanie Crofts, Dr. Bingyang Zhang, Dr. Bradley Scott, Jules Chabain, and Abby Weber. Thanks also to the undergraduates who have helped over the years: Valerie Silvano, Evi Malone, Catherine Koterba, Jonathan Tinoco, and Rae Van Kanegan.

Thanks to my doctoral committee members, Drs. Sandy Kawano, Charles Roseman, and Andy Suarez. Sandy really took me under her wing as I began attending the Society of Integrative Biology conferences and has provided invaluable feedback on salamanders and biomechanics. Charles has made me ask the hard questions about evolution, while helping to remind me to pace myself on the Ph.D. journey. Andy was so helpful in learning to navigate the University of Illinois system when I first began, and I enjoyed our conversations about careers and the future of the profession.

Finally, I would like to thank the friends and family that have provided boundless emotional support, both near and afar. To my parents Joe and Elizabeth Darcy, and brother Joe Darcy, who have understood why I needed to do work while visiting for the holidays. To all the friends I have made over the years and kept me grounded. To Scott and Carla Andresen, for reminding me of the bigger picture outside of the narrow view of graduate school. And finally, to Will Andresen, for always being by my side and being my biggest champion.

This dissertation was supported by funding from the School of Integrative Biology, the Department of Evolution, Ecology, and Behavior, and a GAANN Fellowship from the

Department of Education. Travel to present research was supported by the Society of Integrative and Comparative Biology. This work made use of equipment at the Imaging Technology Group, Beckman Institute for Advanced Science and Technology and Materials Research Laboratory, Grainger College of Engineering, UIUC.

TABLE OF CONTENTS

CHAPTER 1: INTRODUCTION 1

CHAPTER 2: MORPHOLOGICAL VARIATION IN THE VOMER OF AQUATIC AND TERRESTRIAL SPELERPINI SALAMANDERS 8

CHAPTER 3: CONVERGENCE IN CRANIAL MORPHOLOGY AMONG AQUATIC AND TERRESTRIAL SALAMANDERS OF THE FAMILIES AMBYSTOMATIDAE AND PLETHODONTIDAE 21

CHAPTER 4: MATERIAL PROPERTIES OF CRANIAL BONE IN THE MEXICAN AXOLOTL (*AMBYSTOMA MEXICANUM*) 40

CHAPTER 5: FUNCTIONAL PERFORMANCE OF THE LOWER JAW VARIES ACCORDING TO HABITAT TYPE IN TWO SALAMANDER FAMILIES 54

CHAPTER 6: CONCLUSIONS 68

REFERENCES 69

APPENDIX A: SPECIMEN DATA SOURCES FOR CHAPTER 2 76

APPENDIX B: SPECIMEN DATA SOURCES FOR CHAPTER 3 78

CHAPTER 1: INTRODUCTION

Background

The earliest tetrapods faced the challenge of co-opting structures that arose in aquatic ancestors for terrestrial life. For example, suction feeding is ineffective on land. Subsequently, skull morphology had to change to accommodate new feeding behaviors, while retaining functions including protecting the central nervous system, housing sensory organs, and performing other tasks such as burrowing. Modern salamanders present an interesting parallel with early tetrapods, as many have biphasic lifecycles and must transition from aquatic to terrestrial feeding. Additionally, unlike most tetrapods, the skulls of salamanders have a significant cartilage component (Rose, 2003). Pliable material would appear ill-suited for the animal's mechanical demands, as salamanders use their heads for prey acquisition, intraspecific combat, and burrowing. Understanding the mechanical demands of a biphasic lifecycle may yield interesting conclusions about the utility of flexible support tissues as well as insight on the ancestral transition from water to land in the first tetrapods.

Salamander Feeding and Influence on Skull Shape

Salamanders are carnivorous, both as larvae and as adults. Among aquatic individuals, stomach content is a gross representation of the prey available in the microhabitat "suggesting that little dietary specialization occurs" (Duellman and Trueb, 1986). Deban and Wake (2000) classified two common feeding patterns and named them after the morphologies they correlate with: "ancestral" and "direct-developer." In the ancestral condition, aquatic larvae suction feed and terrestrial adults use tongue protraction. Though gill and caudal fin morphology vary in

response to the energy of the water system, presenting a gradient from pond to stream to mountain brook habitats, feeding behavior of larval salamanders appears identical among these forms (Deban and Wake, 2000). In direct-developing, terrestrial salamanders, the larval stage is by-passed or too short for the individual to feed, and individuals are born able to use tongue protraction.

All terrestrial species have been observed to use tongue protraction, though jaw capture has been documented in certain groups. Typically prey items are small enough to be brought fully into the oral cavity. However, biting is necessary for immobilizing large prey and has a role in intraspecific aggression (Wake and Deban, 2000). Jaw capture has been observed in Ambystomatidae, Salamandridae, and Plethodontidae, particularly when the tongue fails to apprehend the prey (Larsen and Guthrie, 1975; Miller and Larsen, 1990; Wake and Deban, 2000). Some semiaquatic species of plethodontid (*Desmognathus quadramaculatus*) and hynobiid (*Salamandrella keyserlingi* and *Batrachuperus persicus*) use jaw prehension in water, while the fully aquatic *Desmognathus marmoratus* use either tongue or jaw prehension in water (Schwenk and Wake, 1993). Wake and Deban (2000) note that quantitative kinematic studies are "limited to only a few species", conducted under artificial conditions, and use "limited, sometimes unnatural, prey", while behavior modulation is described in only a couple species "even though most species feed on a diversity of prey and under a variety of conditions."

It was long thought that jaw prehension was the extent of prey processing in lissamphibians, with the singular exception in the plethodontid *Desmognathus* in which they deliver strong bites by rhythmically bobbing their heads while holding prey in their jaws (Dalrymple et al., 1985; Deban and Richardson, 2017; Larsen and Beneski, 1988; Schwenk and Wake, 1993). However, a similarly elaborate behavior has recently been observed in the

salamandrid *Triturus carnifex* (Heiss et al., 2019). In this case, prey was manipulated by the tongue in a loop (antero-dorsal to ventro-posterior), "rasping" it against the vomerine teeth on the roof of the mouth. Complex, three-dimensional chewing has also been observed in sirenid salamanders (Schwarz et al., 2021). Vomerine teeth are common in all salamander families, but it is unclear at this time if other species use them for similar prey processing; rhythmic behaviors have also been observed in ambystomatids, but the transport cycles are different than in salamandrids (Heiss et al., 2019).

Cranial shape is highly variable among salamanders (Herrel et al., 2019) and likely linked to diet. For example, in comparing two plethodontid genera, Martof and Rose (1962) interpret the greater flexibility and elongation of *Gyrinophilus* skulls as an adaptation for eating other salamanders compared to the robust skulls of *Pseudotriton*, which use their heads to dig and feed on earthworms, insects, and relatively smaller salamanders. Food preference may also play a role in the morphology of the ventral aspects of the skull, at least in European newts. Variability of the tooth-bearing ventral bones in *Triturus* and *Lissotriton*, which make direct physical contact with prey items, is not correlated with phylogenetic relationships; in contrast, the dorsal bones in the same species have morphology correlated with phylogenetic relationships (Ivanović and Kalezić, 2010; Ivanoić et al., 2012). Additionally, morphological differences in overall head shape associated with dietary partitioning has been observed in population contact zones of Appalachian *Plethodon* species (Adams and Rohlf, 2000; Maerz et al., 2006, Adams, 2010, Paluh et al., 2015).

Aquatic salamanders demonstrate how difficult it is to predict function or behavior from form alone. Lauder and Reilly (1996) used character mapping to test for correlations among physiological function, structure, and behavior in aquatic salamanders of the genera *Ambystoma*,

Cryptobranchus, *Necturus*, and *Siren*. They found no clear relationships among these characters and concluded that the analysis of a single level alone (function, structure, or behavior) is insufficient to describe the design of salamander feeding apparatus, and that to predict behavior or function from structure would be "effectively impossible". However, analyses of primates, pigs, crocodilians, and bats suggest that different regions of the skull are optimized for different functions (Ross and Metzger, 2004; Santana et al., 2012). The salamander feeding apparatus is not responsible for a single function or behavior. The jaw suspension also supports gill arches, which themselves can vary morphologically based on the velocity of the water. Jaws are used for interspecific combat and mating behaviors. Skull profile may be constrained by hydrodynamic properties of their aquatic habitat. The analysis of form and function therefore requires a multivariate approach.

Biomechanical Models

Biomechanical models allow us to test hypotheses that would be difficult or impossible to test physically. An increasingly common technique to study the relationship between form and function is the combination of geometric morphometrics (GM) and finite element analysis (FEA) (Polly et al., 2016). GM allows one to quantify shape changes, whereas FEA allows one to test the functional consequences of these shape changes. Phylogenetic comparative methods can then be used to evaluate how these form-function relationships change over evolutionary timescales. When a morphological structure performs multiple functions, as in turtle shells studied by Stayton (2011), a performance landscape can propose potential evolutionary trade-offs. For example, Stayton (2011) found that functional trade-off among Emydidae turtles between mechanical strength and hydrodynamic performance. By visually mapping different adaptive

peaks for different functional demands, one can propose explanations for unoccupied areas of morphospace (Stayton, 2011) or hypothesize how selective pressures have changed over time by incorporating fossil taxa (Polly et al., 2016).

Previous studies have used salamanders as models for early tetrapod evolution (see Fortuney et al. 2015; Fortuny et al., 2016; Fortuny et al., 2017; Konietzko-Meier et al., 2018; Gruntmejer et al., 2019). FEA can be useful in cases where absolute accuracy of the model is less important than the relative abilities of structures to withstand forces Dumont et al., 2009). Because the accuracy of biomechanical models cannot be validated for extinct taxa, the quality of the model inputs is important. The steps in the FEA are: creating a geometric model, assigning material properties to the geometry, assigning boundary conditions to prevent displacement, and applying a force (Panagiotopoulou, 2009). The outputs of the analysis are a visualization of deformation along the geometry and values of maximum strain. The morphological variation observed in aquatic and terrestrial species will be investigated in the first two chapters and will supply the input geometries. The third chapter will focus on characterizing salamander cranial bone properties, which has not yet been reported in the literature. The most useful material property used for constructing biomechanical models, which has not yet been characterized in anamniote skull bone, is Young's modulus. Young's modulus is defined as the ratio of stress to strain and gives a sense of how deformable the material is. Materials with higher Young's modulus values may be thought of as being stiffer. Previous work concerning amphibian skull biomechanics have used different workarounds to perform comparative studies without access to material property values of anamniotes. Zhou et al. (2017) compared a range of Young's modulus values (0.0665 GPa, 1.7 GPa, 3.35 GPa, 5.0 GPa and 6.0 GPa) in their work on Siberian salamander (*Salamandrella keyserlingii*) skulls. Kleinteich et al. (2012) built caecilian skull

models using a modulus of 10 GPa, based on experiments on *Uromastyx* lizards (i.e., Moazen et al., 2008; Moazen et al., 2009). Most other amphibian skull biomechanical models, whether looking at extant Chinese giant salamanders (*Andrias davidianus*) or Late Triassic temnospondyls, use a modulus of 6.65 GPa based on Currey's (1987) characterization of the frontal bone of *Crocodylus* (see Fortuney et al. 2015; Fortuny et al., 2016; Fortuny et al., 2017; Konietzko-Meier et al., 2018; Gruntmejer et al., 2019).

Study Taxa

This dissertation seeks to understand the relationship between form and function associated with the evolution of secondarily aquatic species of salamanders. My research focuses on two groups of North American salamanders: the family Ambystomatidae (32 spp.) and the Plethodontidae tribe Spelerpini (42 spp.). Both groups include members that have secondarily aquatic species, and the degree to which species are aquatic is variable. Some are facultatively aquatic, where individuals reach sexual maturity in the aquatic larval form without undergoing metamorphosis when conditions on land are unfavorable. Others are obligatorily aquatic, where all members of a species remain aquatic and the ability to metamorphose is functionally absent. All aquatic species of Spelerpini examined here are obligate, while *Ambystoma* includes both obligate and facultatively aquatic species. This provides the opportunity to compare how the land-to-water transition affects skull morphology and performance in two independent lineages that differ in the propensity to remain aquatic as sexually mature adults. Ambystomatidae consists of a single genus, *Ambystoma*, found in Canada, the U.S., and Mexico. Known as the mole salamanders, they are relatively drought-resistant due to their ability to burrow. The plethodontid tribe Spelerpini is comprised of 5 genera (*Eurycea*, *Gyrinophilus*, *Pseudotriton*,

Stereochilus, and *Urspelerpes*). They are found in eastern North America, from Quebec to Texas (Duellman, 1999). As members of the lungless salamander family, they are more dependent on moisture than the ambystomatids. About 85% of plethodontid species are direct developers (Marks, 2000), while ambystomatids are biphasic. Despite their different moisture tolerances, both groups have colonized relatively arid habitats. Neotenic populations of *Ambystoma* are found in the high-elevation lakes of Mexico, and some populations have given rise to permanently aquatic species such as the axolotl (*A. mexicanum*) (Duellman, 1999). In Texas and the Internal Highlands, the plethodontid genus *Eurycea* has colonized cave and spring systems. Most of the aquatic species of *Eurycea* have external morphologies resembling the larval forms of their terrestrial relatives, some aquatic species have a "troglodytic" morphology of reduced eyes and elongated snouts (e.g., *Eurycea rathbuni*).

My dissertation chapters synthesize what is known about the ecomorphological variation in ambystomatid and plethodontid salamanders, introduce the first characterization of salamander cranial bone material properties, and demonstrate if the land-to-water transition leads to different functional performance in the jaw.

CHAPTER 2: MORPHOLOGICAL VARIATION IN THE VOMER OF AQUATIC AND TERRESTRIAL SPELERPINI SALAMANDERS

Abstract

The vomer is an important tooth-bearing cranial bone in the lungless salamanders (Caudata: Plethodontidae) that serves different functional roles in aquatic versus terrestrial feeding. Vomerine tooth rows that run parallel with the maxillary teeth are thought to help grasp prey while expelling water from the mouth, while posterior extensions of the tooth row may help terrestrial taxa bring prey down the throat. I hypothesize that these two general morphological types will correlate with the habitat (aquatic versus terrestrial) of adult salamander. Alternatively, variation in form may be due to taxonomic effects, such that closely related species will have similar vomer morphology regardless of adult habitat. To test this hypothesis, I examined vomer shape on a set of species of the morphologically diverse tribe Spelerpini, in which two of the five genera (*Eurycea* and *Gyrinophilu*s) include both aquatic and terrestrial species. Data were collected using micro computed tomography (microCT) scans from specimens from the Field Museum of Natural History and the Illinois Natural History Survey; additional data was obtained from public online repositories including Morphosource.org. Two-dimensional geometric morphometric analyses were performed to capture shape variation of both the vomer and the vomerine tooth row. I found clear separation between aquatic and terrestrial taxa, with most of the variation due to differences in the vomerine tooth row. Differences ascribed to habitat use likely correspond to feeding behavior, and the functional role of the vomer in prey processing warrants further investigation in this family.

Introduction

Most plethodontid salamanders exhibit niche conservatism, where species retain ancestral niches and associated morphological traits. Speciation under this regime typically occurs due to geographic or environmental barriers. However, this pattern of speciation is not well-supported by previous studies of the salamander tribe Spelerpini (Vieites et al., 2011). Spelerpini consists of two lineages: a clade including the genera *Stereochilus*, *Pseudotriton*, and *Gyrinophilus*, and a sister clade consisting of *Eurycea* and the monotypic *Urspelerpes*. The speciation of *Eurycea* has been described as an adaptive radiation with species filling different ecological roles (Wray and Steppan, 2017). The genus *Eurycea* originated in the Appalachian Highlands and expanded into unoccupied niches as the Western Interior Seaway retreated, resulting in four geographically distinct clades (Wray and Steppan, 2017). Permanently aquatic, neotenic species independently evolved in three of these four clades (Bonett et al. 2014). The niche lability in *Eurycea* (especially in the neotenic species of the Edwards Plateau) may have been driven by relatively rapid aridification during the Pliocene and Pleistocene (Wray and Steppan, 2017). Climatic changes may also have led to habitat fragmentation and eventual genetic isolation of relatively aquatic species that would later give rise to the cave-dwelling, troglomorphic species. Cave-dwelling and non-cave-dwelling species of *Eurycea* differ significantly in body shape, with cave-dwellers tending towards limb elongation and reduced body and tail size, and terrestrial species with elongation of both the limbs and digits (Edgington and Taylor 2019). Pipan and Culver (2012) hypothesized that these troglomorphic traits resulted from simultaneous relaxation of selective pressures experienced by their surface-dwelling ancestors and directional selection specific to the cave environment. Wake (1966) and Parra-Olea and Wake (2001) also found evidence for parallel evolution of elongate fossorial taxa. In contrast, body morphology of most

other plethodontid salamanders exhibits strong phylogenetic conservatism (Blankers et al., 2012).

The vomer is a tooth-bearing cranial bone present in all living salamander taxa. It sits posterior to the maxilla and forms the anterior portion of the palate (Figure 2.1). In many groups, the vomerine tooth row is contiguous with a row of parasphenoid teeth or a parasphenoid tooth patch that extends posteriorly. The role of these palatal teeth is not clear. Previously, it was thought that palatal teeth served to grip and aid simple manipulation of prey items before swallowing. Prey processing as defined by "mechanical reduction or preparation of food before it is swallowed" (Schwarz et al., 2020) was not believed to exist in extant amphibians (Lauder and Reilly, 1990; Schwenk and Schwenk, 2000). However, new studies on salamander feeding kinematics are challenging this interpretation. Heiss et al. (2019) found that Italian Crested Newts (*Triturus carnifex*) possess a food processing mechanism. Following the initial prey capture, these newts display rhythmic head bobbing and cyclical jaw and tongue movements. They rasp the prey item along the vomerine dentition on the roof of the mouth using their tongues. Schwarz et al. (2020) also observed complex, 3D chewing action in the distantly related Lesser Siren (*Siren intermedia*). It is quite possible that tongue-rasping prey-processing has gone unobserved in many salamander groups, as rhythmic head and jaw or tongue movements have been observed in other species (see Heiss et al, 2019). This study focuses on Lungless Salamanders (family Plethodontidae), which are not currently known to perform prey-rasping food processing. However, it contains the widest diversity of prey-capture methods observed among modern salamanders, is the most species-rich family, and adult individuals have complex palatal dentition including complex parasphenoid tooth patches (Rose et al., 2003). Therefore,

they are a good model group for understanding the interplay of taxonomic relationships and behavior on the overall morphology of feeding apparatuses.

Previous studies examined the relationship of vomer shape, taxonomy, and ecology. Wake (1966) described three distinct vomerine morphologies observed in adult, terrestrial plethodontid salamanders, and represents the most thorough description of this bone to date. He found discrete morphological characters of the vomer that could potentially distinguish genera. This suggestion was supported by a geometric morphometrics analysis by Darcy (2015). However, a study by Jia et al. (2002) that included both terrestrial and aquatic species among cryptobranchid and hynobiid salamanders (Cryptobrancoidea) determined that morphology is constrained by habitat-determined feeding mechanics (i.e., feeding in terrestrial, semi-aquatic, or aquatic habitats) among living and extinct salamander species.

I characterized vomer morphology in the lungless salamander tribe Spelerpini to determine if morphology is taxonomically conserved or driven by ecology, as in Cryptobrancoidea salamanders. This clade of lungless salamanders includes both terrestrial and secondarily aquatic species, presenting an opportunity to consider convergence. I hypothesized that generalized feeding behavior will predict vomer morphology regardless of taxonomic affinity, but that *Eurycea* will occupy a larger area in morphospace than the rest of Spelerpini.

Methods

Data Acquisition

The vomer is a generally flat element, with most of the morphological variation evident in the ventral plane, suitable for two-dimensional analysis (Figure 2.1). The dataset (n=28) is a combination of photographed and three-dimensional micro-CT scans. Photographed specimens

(n=5) were taken using a Lexar microscope camera at the East Tennessee State University Vertebrate Paleontology Laboratory (ETVP) (Darcy, 2015). Bones were oriented such that the medial margin of the bone was parallel to the vertical axis of the view finder and the flat palatal surface was perpendicular to the Z-axis. Half of the scan data were drawn from Phenome10k.org (n=1l; Creative Commons Attribution-Noncommercial 4.0 International License; Goswami, 2015). The remaining scan data (n=11) were generated from Field Museum of Natural History specimens that I scanned at the Imaging Technology Group of the Beckman Institute for Advanced Science and Technology. Raw scan data was sectioned using Avizo (ThermoFischer Scientific) and exported as .stl files. All three-dimensional data were edited in Geomagic Wrap 2017 (3D Systems, Rock Hill, South Carolina) to remove the lower jaw allowing a full view of the vomer. Within Geomagic Wrap, crania were oriented so that the palatal view was centered on the screen and the cranium was oriented flat with respect to the screen. 2D screenshots were captured so scan data could be incorporated into the photographed dataset.

Geometric Morphometrics

Analysis of vomer shape variation was based on landmarks and sliding semi-landmarks placed on the 2D images using tpsDIG2 software (Rohlf, 2013a) and appended using tpsUtil (Rohlf, 2013b). I defined 6 landmarks of analogous anatomical locations that could be reliably placed on all study specimens (Figure 2.1). One curve capturing the vomerine tooth row was defined by three sliding semi-landmarks evenly distributed along the line, anchored by the fixed landmarks 1 and 6 at either end.

Landmarks were aligned with a Generalized Procrustes analysis in the R package geomorph (geomorph version 3.2.0, Adams et al., 2019; R version 3.6.2). The analysis is a least-

squares method that superimposes, rotates, and scales landmarks, allowing for shape comparisons while removing size, position, and orientation of the original image as variables (Rohlf and Slice, 1990). Semi-landmarks were aligned to minimize bending energy. This step generated coordinates for use in principal component analyses (PCA) (Morpho version 2.8; Schlager, 2017). A phylogeny adapted from Jetz and Pyron (2018) (Figure 2) was superimposed onto the PCA plot using the phytools package (phytools version 0.7-90; Revell, 2012) to create a phylomorphospace. The phylomorphospace allows for a visual comparison of morphological variation, where more similar geometries cluster in the figure. The superimposed phylogeny allows us to examine if any clustering is due to ecology or taxonomy.

Results

A principal component analysis of all study taxa separated aquatic taxa and the terrestrial + semi-aquatic taxa along the PC1 axis (Figure 2.3). The first two principal component axes accounted for a cumulative 86.53% of the variation in landmarks among species, with PC1 alone accounting for 79.79% of the variation. PC1 captured the x-coordinate of landmark 2, or the lateral position of the medial-most point of the vomer bone. Terrestrial species had more negative PC1 values, while aquatic species had more positive PC1 values. PC2 accounted for 6.74% of the variance and captures the y-coordinate of landmark 2, or the anterior-posterior position of the medial-most point of the vomer bone. The non-Eurycea species fall in the bottom-left quadrant, with negative PC1 and PC2 values. The semi-aquatic *Stereochilus marginatus* clusters with the terrestrial taxa. Eurycea range between –0.2-0.2 on the PC2 axis but are more widely separated along the PC1 axis according to habitat type. Among aquatic species, there was no separation between spring- and subterranean-inhabiting species.

The phylomorphospace showed that aquatic taxa shift towards more positive PC1 values compared to their terrestrial relatives (Figure 2.4). Terrestrial *Eurycea* species have values more similar to the other genera than to the aquatic *Eurycea* species. The disparity is most evident when comparing sister taxa, specifically: the clade that contains the terrestrial species *E. quadridigitata* and the aquatic species *E. sosorum*, *E. latitans*, *E. neotenes*, and *E. waterlooensis*; and the clade that contains the terrestrial species *E. cirrigera, E. lucifuga,* and *E. bislineata* as well as the aquatic *Haideotriton wallacei*. *Eurycea spelaea* is the outgroup for all other *Eurycea* species in this phylomorphospace but still forms a cluster with other aquatic species.

Discussion

These results support the hypothesis that vomer morphology correlates with generalized feeding behavior (aquatic suction feeding vs terrestrial feeding strategies) rather than taxonomic affinity. The landmark accounting for most of the observed variation is the medial-most point, which was more anterior in aquatic taxa and more posterior in terrestrial taxa, relative to the anterior-most point. In general, aquatic taxa have shorter vomers that bear a tooth row closer to the anterior of the mouth. This aligns with Wake's (1966) classification scheme for vomerine morphology. The aquatic vomerine morphology, with an anteriorly positioned tooth row, is suitable for grasping prey while water is expelled from the mouth prior to ingestion.

I also found that *Eurycea* occupies a larger area of morphospace than the rest of Spelerpini, as I also anticipated. It occupies a greater range of both PC1 and PC2 values, but other than the aquatic-terrestrial split along PC1, there is not an evident pattern separating spring salamanders that live closer to the surface from the subterranean species. Wray and Steppan (2017) hypothesized that ecological shifts within *Eurycea* should correlate with morphological

variation, and that the morphology of this genus would differ greatly from other Spelerpini taxa. Additionally, Wray and Steppan found that neotenic *Eurycea* in the Edwards Plateau geographic clade (including *E. latitans, E. neotenes, E. sosorum,* and *E. waterlooensis*) experience a different evolutionary rate regime than other Spelerpini salamanders, resulting in an increased diversification rate. The results of this study on vomer morphology suggest a relatively conservative morphospace for most Spelerpini, with *Eurycea* occupying a more expansive region of morphospace.

This study also found greater morphological variation in the Edwards Plateau clade (Figure 2.4), consistent with an increased evolutionary rate correlated with morphological change. In a similar study, Capshaw et al. (2019) found that inner ear variation was also greater in the cave dwelling *Eurycea*, and this was attributed to diverse microhabitat usage. It is unclear if vomerine morphology is also influenced by microhabitat usage, and this uncertainty is exacerbated by the difficulty in observing natural feeding behaviors. It is also possible that the greater observed morphological variation is due to relaxed constraints associated with subterranean environments. For example, the Austin Blind Salamander (*E. waterlooensis*) has an extreme troglodytic morphology, with an elongated snout, reduced eyes, and long limbs for foraging on the substrate. Rather than locating prey visually, as is typical in most other salamanders, cave dwelling *Eurycea* are thought to use neuromasts on the face to sense water flow (Soares and Niemiller, 2020). Like many other subterranean species, cave salamanders develop a “duckbill” rostrum, which may be a secondary consequence of eye reduction and may influence the shape of all cranial bones.

Terrestrial *Eurycea* tended to have slightly lower PC1 and slightly higher PC2 values than the other terrestrial genera, and future work should focus more closely on the terrestrial

species to see if different prey processing behaviors are present and influence vomerine morphology. Different evolutionary rate regimes in *Eurycea* relative to other Spelerpini taxa, coupled with historical range expansions into unoccupied niches, may have facilitated the evolution of the complex prey processing behaviors recently observed in other salamander groups.

Conclusion

Much work is left to do in establishing prey processing behaviors in salamanders and what role the vomerine dentition plays. Novel vomerine morphologies may allow animals to exploit different prey sources and expand into new niches. This study supports the hypothesis that the aquatic salamanders in the Edwards Plateau clade of *Eurycea* experienced increased morphological variation correlated with an increased evolutionary rate. It also emphasizes the differences between aquatic and terrestrial salamanders that feed under very different biomechanical conditions. These observations of the habitat's correlation with environment call for a broader study of comparative morphology in secondarily aquatic species and their terrestrial relatives, as well as material and direct biomechanical analyses of shape associated with this evolutionary transition.

Figures

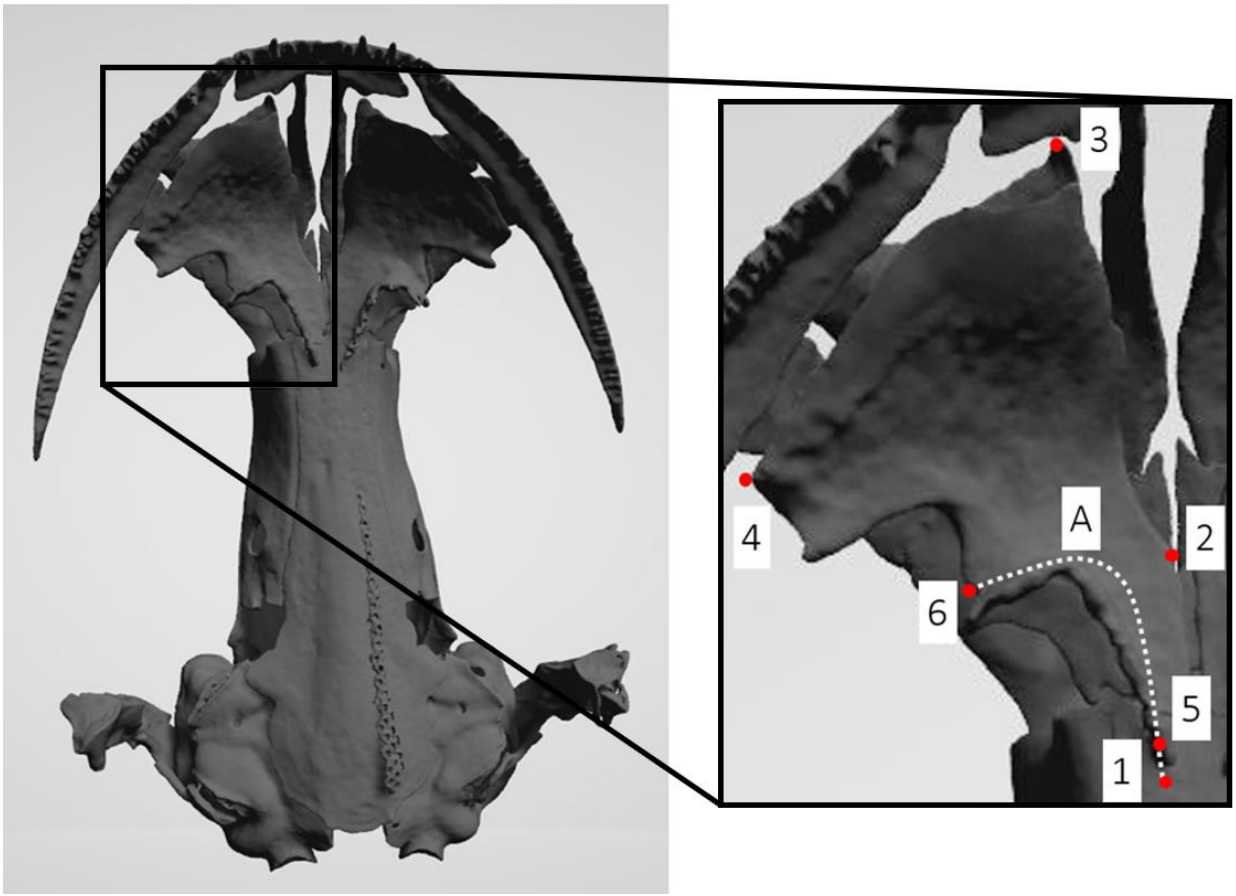

Figure 2.1. Location of the vomer bone and the placement of landmarks that were used in the present study. Left, a ventral view of a *Eurycea lucifuga* skull (BMNH 1957.1.7.86). The black box and call-out image are of the right vomer bone. The location for landmark placement is demonstrated on the right. Landmarks used are: 1, posterior point; 2, medial point; 3, anterior point; 4, lateral point; 5, base of the medial-most tooth; 6, base of the lateral-most tooth. Three sliding semi-landmarks were placed on Curve A, which follows the tooth row along the base of the teeth, anchored on either side by landmarks 1 and 6. Ventral view, where top of page is anterior. Scale bar = 1cm.

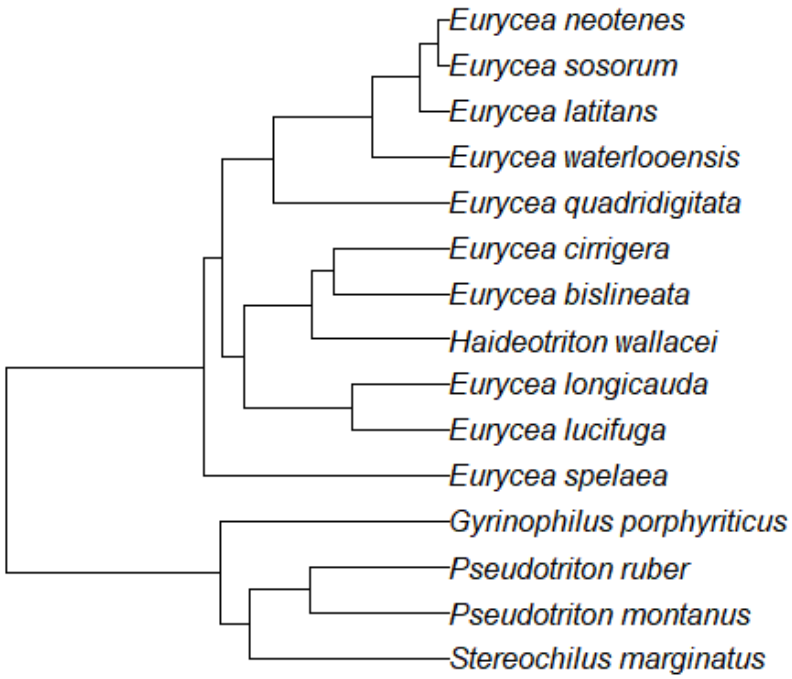

Figure 2.2. A subset of the phylogeny available in Jetz and Pyron (2018) was used to create a phylomorphospace incorporating phylogeny into the results of the geometric morphometrics analysis. Pictured are the phylogenetic relationships of the included taxa, generated in R. The two major clades of tribe Spelerpini are *Eurycea+Haideotritoin* and *Gyrinophilus+Pseudotriton+Stereochilus.*

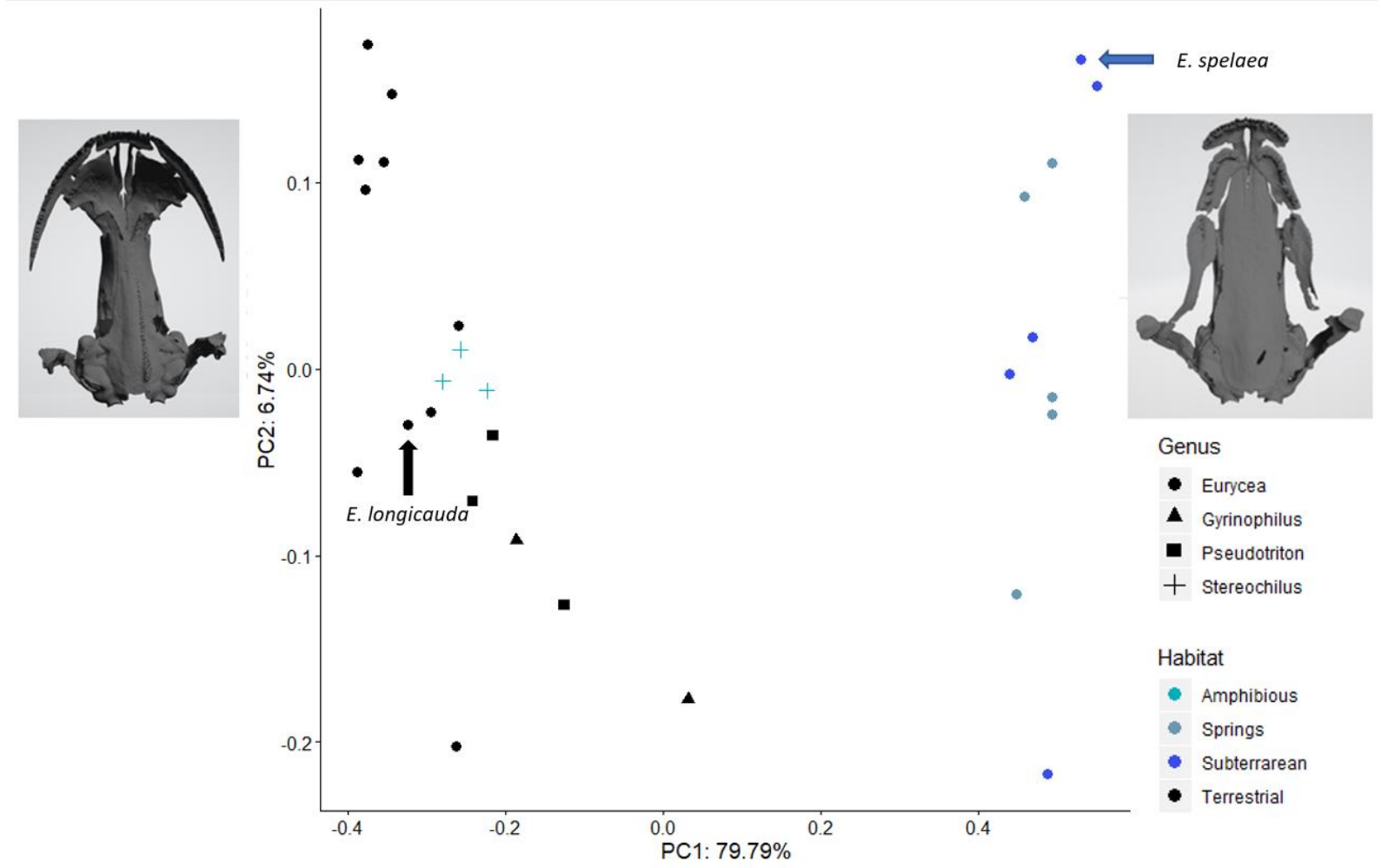

Figure 2.3. Principal component analysis results for the geometric morphometrics analysis including the full dataset of study taxa. A cumulative total of 86.53% of total variation is represented in the first two axes. The first principal component axis captures 79.79% of the observed variation, and the second principal component axis captures 6.74% of the observed variation. Genus is indicated by datapoint shape and habitat is indicated by color.

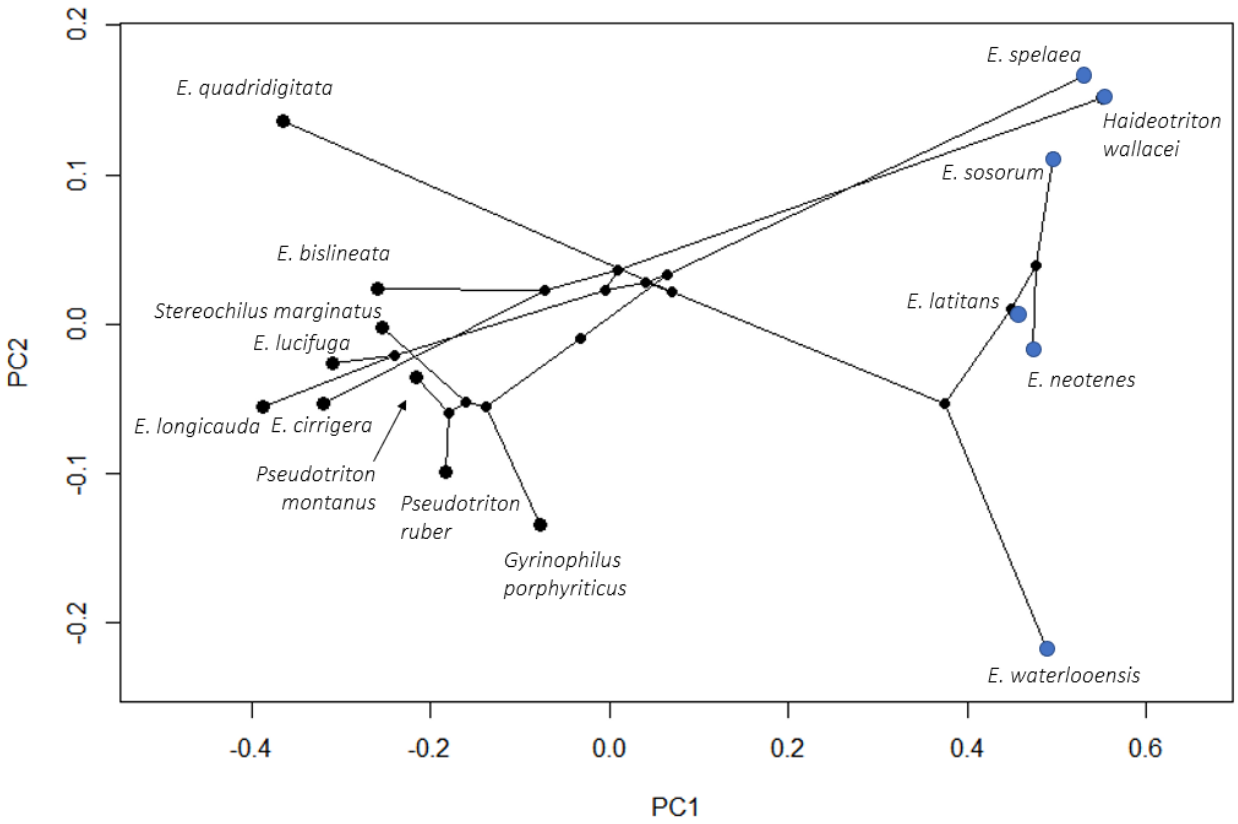

Figure 2.4. Phylomorphospace that includes the subset of taxa with available phylogenetic information (Figure 2.2) projected onto the morphospace (Figure 2.3). Habitat is indicated by color: light blue circles, aquatic; black circles, terrestrial. Aquatic species have higher PC1 values regardless of taxonomic affiliation.

CHAPTER 3: CONVERGENCE IN CRANIAL MORPHOLOGY AMONG AQUATIC AND TERRESTRIAL SALAMANDERS OF THE FAMILIES AMBYSTOMATIDAE AND PLETHODONTIDAE

Abstract

While aquatic salamander skull morphology has been used as an example of the difficulty of form to function mapping, previous work did not consider evolutionary history in their analyses. This study examines morphological patterns in secondarily aquatic salamanders in a broader context that includes their terrestrial relatives. Geometric morphometric methods are applied to a dataset of 47 crania from Ambystomatidae and Plethodontidae salamanders that live in aquatic and terrestrial habitats to build a phylomorphospace. I found that aquatic taxa show a shift in morphospace relative to terrestrial species that corresponds to changes in the jaw suspension apparatus that is involved in suction feeding. This shift is observable in the context of phylogenetic history, demonstrating the importance of evolutionary history when searching for cases of convergence.

Introduction

There is not always a tight match between structural and mechanical function in tetrapod skulls. Broad correlations between morphology and performance can be observed at coarse-scales (e.g., aquatic or terrestrial; hard or soft prey) and at fine-scales (within physiological tissues) but the same is not always true for intermediate scales at the intraspecific or interspecific levels (Lauder, 1996). For example, it is “often stated” that skulls are should be optimized to resist feeding forces (Ross and Metzger, 2004), but when examining bone strain gradients across

skulls, it appears different regions are optimized for different functions in primates, pigs, and crocodilians (Ross and Metzger, 2004) and potentially bats (Santana et al., 2012). Aquatic salamanders have been used as an explicit example of how difficult it is to predict function or behavior from morphology alone. Lauder and Reilly (1996) used character mapping to determine if there were correlations among physiological function, structure, and behavior in aquatic salamanders of the genera *Ambystoma*, *Cryptobranchus*, *Necturus*, and *Siren*. However, superficially similar morphologies can be achieved by different non-adaptive processes. In salamanders, a major source of phenotypic variation appears to allometry and heterochrony. These appear to be the dominating patterns in salamander phenotypic variation from the species level to the emergence of the Batrachia (salamanders+frogs). Allometry is the differential rate of growth of different body parts, often due to scaling rules (e.g., a doubling in height requires a quadrupling of limb bone thickness). Heterochrony (*sensu lato*) is an alteration of the timing of developmental events (Jablonski, 2000). Heterochrony can take the form of paedomorphosis in salamanders, which is more akin to a binary switch (metamorphose or don't metamorphose) than a change in developmental timing. Paedomorphic salamanders continue developing in an aquatic habitat, leading to an overall phenotype that combines larval and adult traits. In contrast, neotenic salamanders experience delayed somatic development and consequently reach sexual maturity while retaining larval traits (Iordansky, 2005). Therefore, two heterochrony mechanisms can lead to the same broad phenotype and apparent convergence: a sexually mature aquatic form in an otherwise terrestrial lineage.

The far-reaching effects of heterochrony mean that changes to entire phenotypes can be due to the selective pressure on habitat (i.e., to become secondarily aquatic). Paedomorphic plethodontids and neotenic ambystomatids have very different skull shapes, but that is due to

how they achieved secondarily aquatic states, and not necessarily due to different selective pressures on feeding, swimming, etc. When heterochronic traits become fixed and a species becomes obligatory paedomorphic or neotenic, rates of evolution can increase due to lower gene flow with aquatic neighbors (Jablonski, 2000). This has led to divergent phenotypes among six species of *Ambystoma* of which five are obligatory neotenic and one is facultatively neotenic (Shaeffer, 1984). Fixation may happen if the trait under selection in ambystomatid salamanders is phenotypic plasticity itself, as proposed by Levis and Pfennig (2018). Facultative neoteny is beneficial in the arid American Southwest; *Ambystoma tigrinum* is the only native salamander species in this region because generations born in particularly dry years can reproduce in their breeding pond. Once neoteny is fixed, isolated populations are subject to genetic drift. It has been estimated that in most salamander lineages, it takes over 10 million years for a lineage to completely lose its metamorphic capability (i.e., metamorphosis when artificially exposed to thyroid hormones), and that paedomorphosis/neoteny is reversible in living plethodontid and ambystomatid species but irreversible in families that have been aquatic since at least the Cretaceous (Amphiumidae, Cryptobranichidae, Proteidae, and Sirenidae) (Bonett et al,. 2014).

Lauder and Reilly did not consider evolutionary history in their demonstration of character mapping, which may be the direct cause of their inability to map structure to function. The importance of this consideration was demonstrated by Stayton (2006), in a study on the evolution of herbivory in lizards. He found that the crania of herbivorous lizards exhibit similar shifts in morphospace relative to their carnivorous relatives (indicating larger orbits, shorter snouts, and higher temporal regions than their relatives). However, because these shifts were relative to sister taxa, and all herbivorous lizard crania do not cluster together, this convergence was long overlooked by those ignoring evolutionary history. In the present study, I will seek

similar overlooked signals of convergence in cranial morphology among aquatic and terrestrial salamanders in the families Ambystomatidae and Plethodontidae.

Taxa Selection

Ambystomatids are a monogeneric family of mole salamanders (Ambystoma) widely spread through North America and northern Central America in areas receiving at least 50 cm of precipitation a year (Duellman and Sweet, 1999). The *Ambystoma tigrinum* species complex in the Trans-Mexican Volcanic Belt region has given rise to several neotenic species such as the Mexican axolotl (*Ambystoma mexicanum*). There are 19 currently recognized species in the complex (Everson et al., 2021). Their metamorphic capabilities range from obligate metamorphs to obligate neonates, with some species showing an equal propensity to change or remain in the larval form (Table 1). Diversification within this group appears to be driven by geography rather than life history changes; gene flow is present among all species except *A. dumerilii*, and most speciation occurred within the last 1 million years (Everson et al., 2021).

A different evolutionary pattern explains the diversification of aquatic salamanders in the plethodontid tribe Spelerpini. Brook salamanders (*Eurycea* spp.) speciated during an adaptive radiation into niches exposed as the Western Interior Seaway receded (Wray and Steppan, 2017). Permanently aquatic, paedomorphic species independently evolved in three of the four major *Eurycea* clades and include species that live at the surface as well as cave-dwelling, troglomorphic species with elongate rostra and reduced eyes (Bonett et al. 2014) (Table 3.2). Pipan and Culver (2012) hypothesized that these troglomorphic traits resulted from simultaneous relaxation of selective pressures experienced by their surface-dwelling ancestors and directional selection specific to the cave environment.

These two salamander families produced secondarily aquatic species through different developmental pathways. The literature uses the terms “neoteny” and “paedomorphic” loosely, but they are different forms of heterochrony that can result in an animal that can sexually reproduce while retaining larval traits. In neoteny, somatic development is delayed so that larval traits are retained at sexual maturity. This is what occurs in aquatic *Ambystoma*. In paedomorphosis, somatic cells develop at a normal rate and germ cells develop at an accelerated rate. This results in a combination of larval and adult physical traits at sexual maturity. This is what occurs in aquatic *Eurycea* (Plethodontidae) (Iordansky, 2005).

Despite differences in life history, I hypothesized that the two families will show some degree of convergence in cranial morphology. Lauder and Reilly (1996) were searching for classical convergence, where there is an ideal peak in a morphospace that all aquatic taxa gravitate towards (Figure 3.1, A). Instead, they claim aquatic salamanders show no convergence in a morphospace (Figure 3.1, C). However, without comparing the aquatic species with terrestrial relatives, they could not know if there was a relative shift along a particular vector that may be associated with a habitat shift (Figure 3.1, B). This was the observation made by Stayton (2006) in herbivorous lizards, where phylogeny controlled most of a taxon’s location in morphospace, but herbivorous taxa showed a similar shift away from their carnivorous relatives due to similar morphological changes related to diet.

Cranial morphology changes greatly during post-hatching development in salamanders, with the presence and absence of bones serving as good indicators of larval stage (Nye et al., 2003; Rose et al., 2003). Because aquatic ambystomatids and plethodontids exhibit different heterochrony patterns, it is unlikely that they will exhibit classical convergence patterns;

however, it is possible that aquatic species will shift along a similar vector in morphospace away from their terrestrial relatives.

Methods

Data Acquisition

Forty-seven adult individuals representing 32 taxa were included in the study. Three-dimensional shape data was collected from microCT scans of museum specimens from the Field Museum of Natural History and the Illinois Natural History Museum; these were scanned at the Imaging Technology Group of the Beckman Institute for Advanced Science and Technology. The remaining dataset was drawn from the online repositories Morphosource.org and Phenome10k.org. Raw scan data was sectioned using Avizo (ThermoFischer Scientific) and exported as .stl files.

Geometric Morphometrics

Three-dimensional landmarks were placed using Stratovan Checkpoint (Stratovan Corporation, Davis, CA, USA) (Table 3.3; Figure 3.2). Landmarks were selected to reflect homology or analogy between the two families. They were placed on the right side of the cranium, assuming adequate symmetry of the skull. Landmarks were aligned with a Generalized Procrustes analysis in the R package geomorph (geomorph version 3.2.0, Adams et al., 2019; R version 3.6.2). The analysis is a least-squares method that superimposes, rotates, and scales landmarks, allowing for shape comparisons while removing size, position, and orientation of the original image as variables (Rohlf and Slice, 1990). This step generated coordinates for use in principal component analyses (PCA) (Morpho version 2.8; Schlager, 2017). Three PCAs were

conducted: one including all taxa, one with only Ambystoma, and one with only Spelerpini salamanders. A phylogeny adapted from Jetz and Pyron (2018) was superimposed on the all-taxa PCA plot using the phytools package (phytools version 0.7-90; Revell, 2012) to create a phylomorphospace. When there was more than one individual per species, the x and y coordinates for their locations on the PC1 vs PC2 plot were averaged.

Results

A principal components analysis of all study taxa separated all four groups roughly by quadrant along the first two principal component axes, which cumulatively explain 76.0% of the variation observed in the dataset (Figure 3.3). The PC1 axis separates terrestrial from aquatic taxa, and the PC2 axis separates Spelerpini from Ambystoma. PC1 accounts for 61.71% of the variation observed in the dataset. PC1 is driven by the placement of landmark 7 on the quadrate, which is the ventral-most landmark used in the analysis. It captures both the depth of the skull as a whole and the anterior-posterior position of the quadrate bone. Aquatic species have more negative PC1 values, corresponding to an anteriorly directed quadrate. Terrestrial species have more positive PC1 values, with quadrates that point ventrally or posteriorly. PC2 accounts for 14.29% of the variation. This axis is driven by the placement of landmark 6, or the most dorsoposterior point where the two orbitosphenoids join at the rear of the skull.

Figure 3.4 shows the phylomorphospace for the PCA using the whole dataset that includes both families. Aquatic taxa shift away from their terrestrial relatives towards more negative PC1 and PC2 values, which corresponds to a quadrate that juts anteriorly under the cranium, relative to the more ventral or posteriorly oriented quadrates of the terrestrial taxa.

Separate principal component analyses were conducted for each family to see if habitat still separated taxa along the first two principal component axes. For *Ambystoma* crania analyzed independently, the first two principal component axes cumulatively explain 76% of the variation observed in the dataset, with the PC1 axis separating terrestrial from aquatic taxa (Figure 3.5). Figure 3.6 shows the *Ambystoma* phylomorphospace for all species included in Jetz and Pyron's (2018) phylogeny. The analysis using only Spelerpini taxa resulted in a PCA where the first two principal component axes cumulatively explain 90.12% of the variation observed in the dataset (Figure 3.7). The PC1 axis separates terrestrial from aquatic taxa, while PC2 generally separates most *Eurycea* species from the rest of the group. Figure 3.8 shows the Spelerpini phylomorphospace.

Discussion

The largest factor driving separation in morphospace is the position of the ventral point of the quadrate, but that also encompasses differences to the entire jaw suspensory apparatus that also includes the squamosal. This apparatus is heavily involved in suction feeding, which is a behavior generally lost at metamorphosis when terrestrial salamanders switch to tongue or jaw prehension. Separation along the PC1 axis may reflect this fundamental functional difference in prey capture between groups and the biomechanical pressures of living in water. Of note, *Stereochilus marginatus*, a semi-aquatic species that does not perform suction feeding, falls within terrestrial Spelerpini in morphospace.

This may be a key functional performance that drives variation in salamander crania, which could be tested further by including distantly related salamanders that suction feed, such as *Necturus* and *Cryptobranchus* previously included in the model envisioned by Lauder and

Reilly (1996). One aspect not considered by their model was that *Necturus* is a typical suction-feeder, while *Cryptobranchus* utilizes a unique bidirectional suction-feeding mechanism (Heiss et al, 2013). Their model also included Siren, which has recently been discovered to chew (Schwarz et al., 2020). Their form-function relationship may have been stronger if they had this information about these variable aquatic feeding behaviors.

While the present study finds that there is an observable shift in morphospace reflecting habitat use, and correspondingly feeding behavior, there is still room for improvement in establishing this relationship. The groups cluster separately in morphospace; however, the magnitude of the shift in morphospace is greater in the Spelerpini salamanders than in Ambystoma. Speciation occurred more recently among the *A. tigrinum* species complex, and there is still gene flow occurring in all but the most obligate neonate *Ambystoma* (*A. dumerilii*). Without correcting for time, it is unclear if the distance in morphospace between habitat pairs implies anything about a potential morphological "optimum" or directional selection, or if larger morphological differences are due to genetic drift. However, the separate aquatic lineages of Eurycea made a similar shift along PC1 despite many superficial differences (such as varying degrees of cave adaptation), suggesting that at least within families similar heterochronic processes may lead to similar cranial morphologies. For example, the Texas Salamander *Eurycea neotenes* is a surface-dweller that superficially looks like the larval form of terrestrial species. It clusters in morphospace with cave-dwelling species like the Austin Blind Salamander, *Eurycea waterlooensis*, which has reduced eyes and an elongate, up-turned rostrum.

A more robust analysis may consider divergence time. Aquatic *Eurycea* in Texas diverged from other clades 19 million years ago, and they diverged from the lineage including E. spelaea about 29 million years ago (Wray and Steppan, 2017). One could calculate a rate of

morphological change relative to the “ancestral” area of morphospace populated by terrestrial species for each species. However, I would still expect different rates of change in the two families given what is known about their evolutionary history: *Eurycea* exhibited niche lability and exploited new habitats in underground springs, while *Ambystoma* are retaining larval states to withstand arid conditions.

Conclusion

The data support the possibility of using morphology to predict a life history trait if taxa are examined in a comparative sense. Aquatic salamanders in both Ambystomatidae and Plethodontidae are shifted away from their terrestrial relatives along the same axes in morphospace, but the magnitude of the shift differs. This may reflect different divergence times or differing heterochrony mechanisms leading to aquatic forms.

Figures and Tables

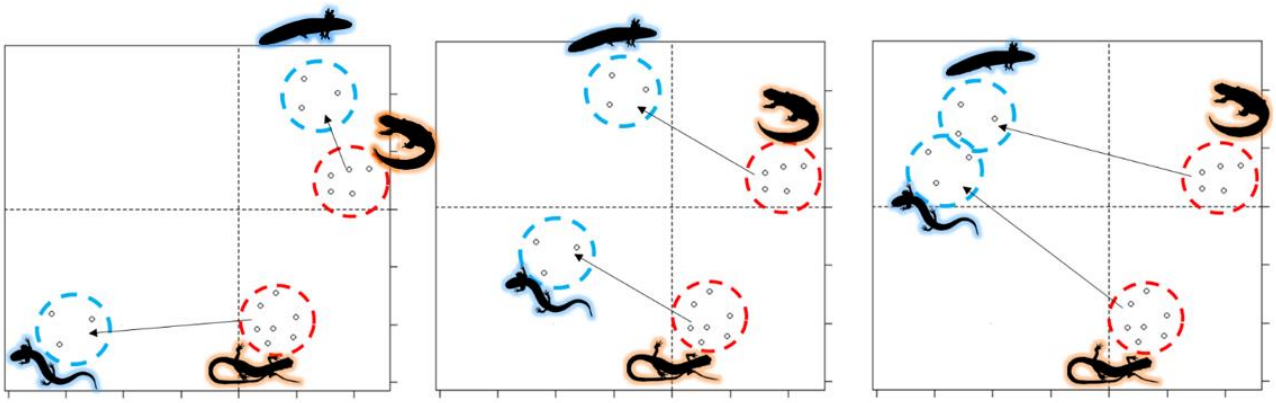

Figure 3.1. Three potential scenarios for mapping cranial morphology in terrestrial (orange) and aquatic (blue) species in morphospace. In scenario A, terrestrial *Ambystoma* (orange, top right) and terrestrial Spelerpini (orange, bottom right) plot far apart, but related aquatic species converge towards a morphological optimum. In scenario B, the aquatic species do not cluster (implying no one optimum for aquatic morphology), but there is a similar vector describing the shift from terrestrial to aquatic forms. In scenario C, there is neither classical convergence nor a similar vector shift.

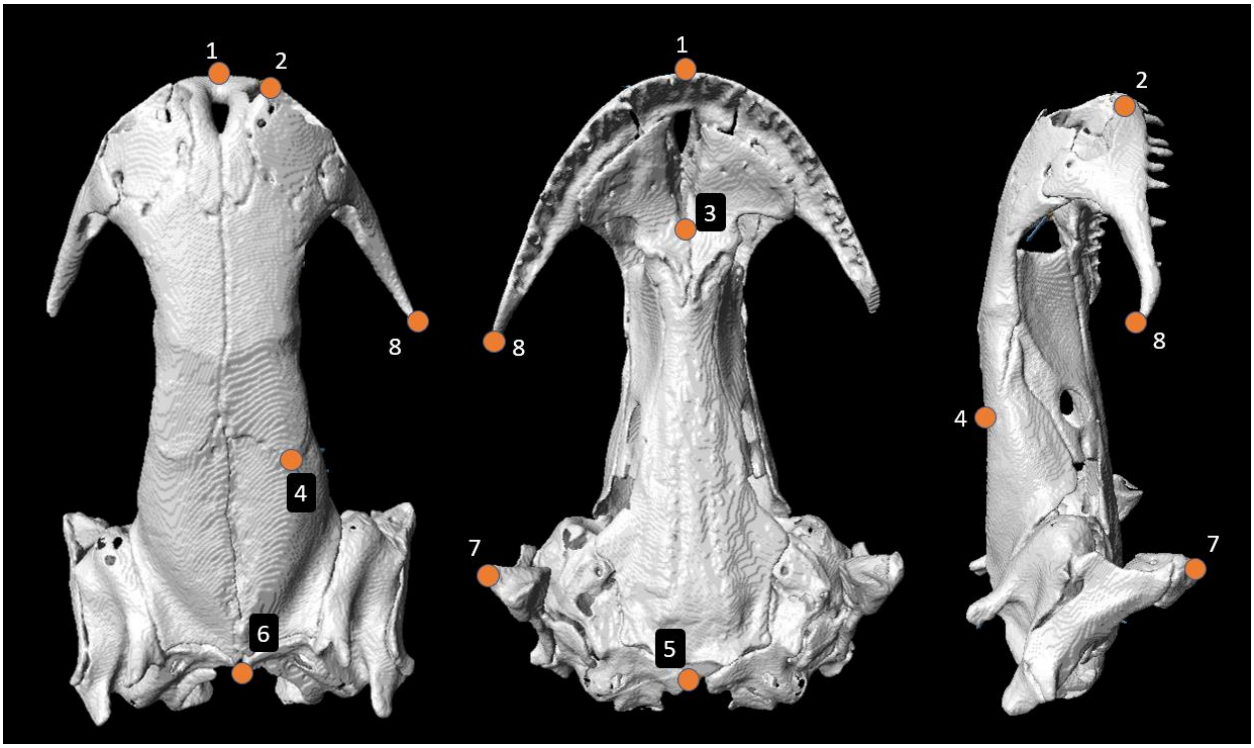

Figure 3.2. Landmark placement on the cranium of *Eurycea cirrigera* in dorsal (left), ventral (center), and right-lateral (right) views. Landmarks were placed along the midline or on the right side of the cranium, assuming adequate symmetry of all skulls. Points capture general proportions of the skull: length, width, and depth. Descriptions of the landmarks are given in Table 3.3.

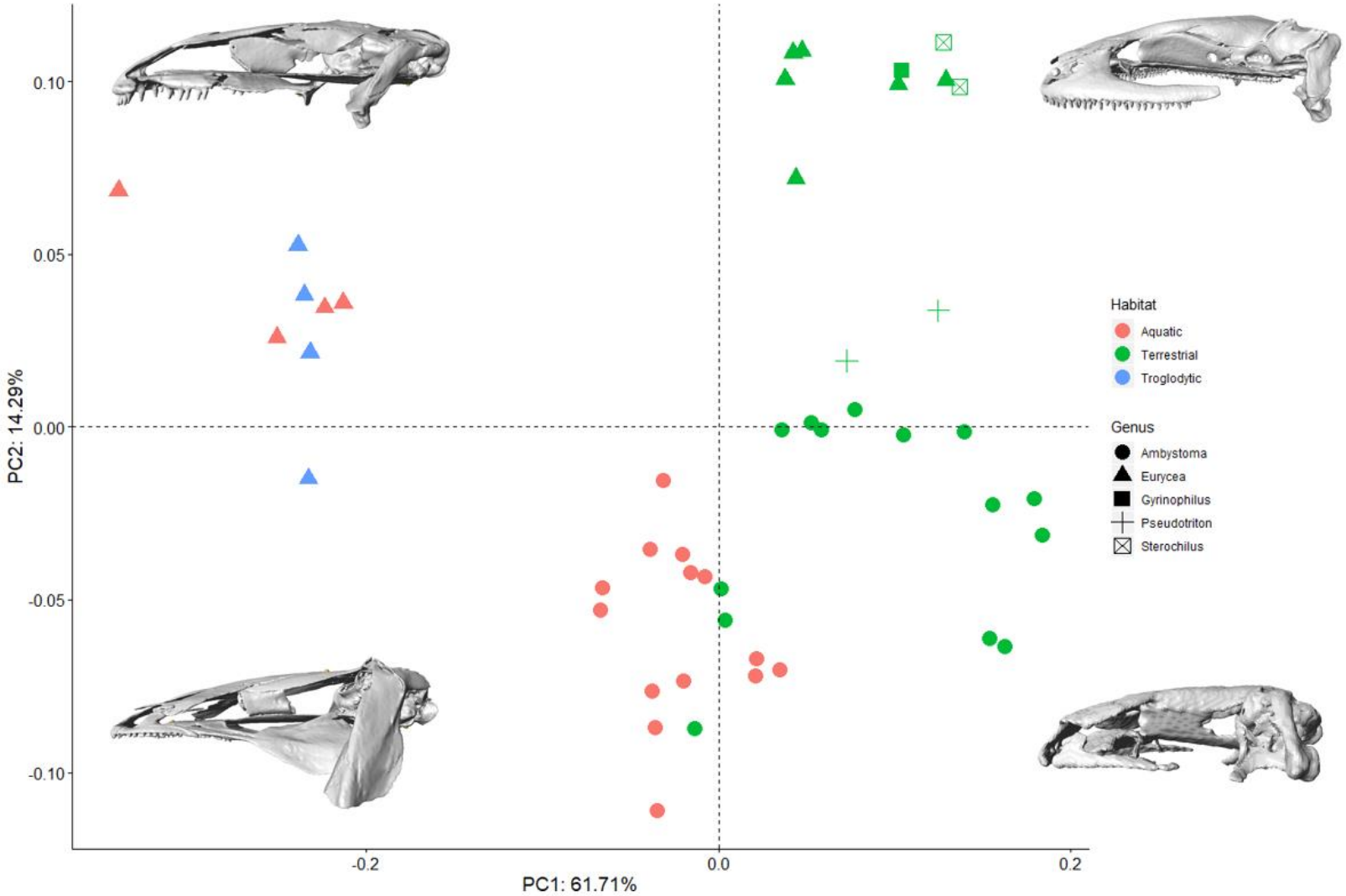

Figure 3.3. Principal component analysis results for all study taxa. The first axis captures 61.71% of observed variation, and the second axis captures 14.29% of observed variation, with 76.0% of all variation represented by the first two principal component axes. The first axis is driven by the antero-posterior position of the ventral end of the quadrate. Habitat is indicated by color and genus is indicated by point shape. Taxa and habitat groups tend to separate into distinct quadrants: top left are aquatic Spelerpini; top right are terrestrial Spelerpini; bottom left are aquatic *Ambystoma*; bottom right are terrestrial *Ambystoma*.

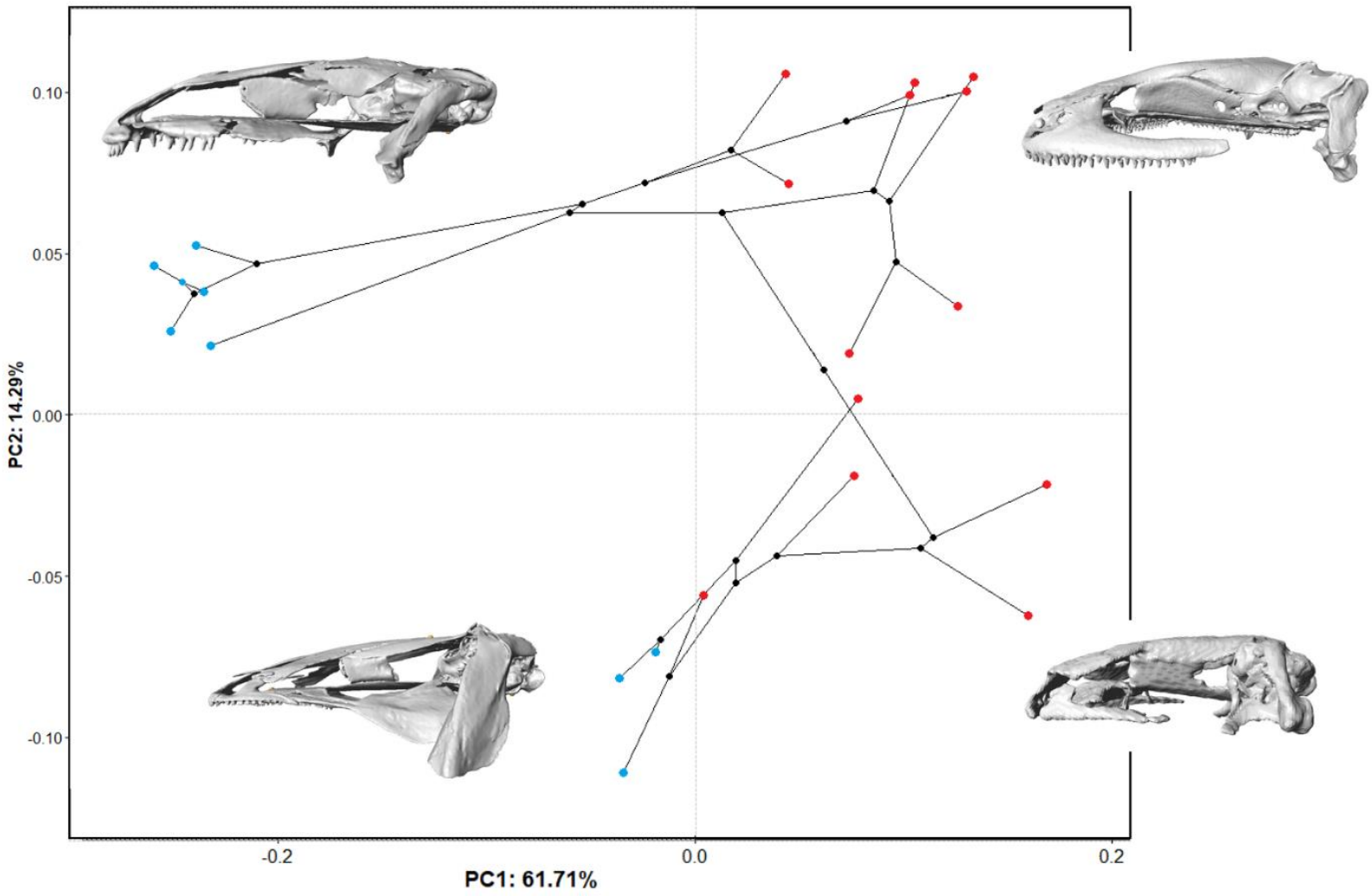

Figure 3.4. Phylomorphospace overlaying phylogenetic relationships on the morphological data. Note the similar shift towards the bottom-left in aquatic taxa (in blue) away from their terrestrial relatives (in red) and away from a hypothesized ancestral condition in the first quadrant. Taxa and habitat groups tend to separate into distinct quadrants: top left are aquatic Spelerpini; top right are terrestrial Spelerpini; bottom left are aquatic *Ambystoma*; bottom right are terrestrial *Ambystoma*.

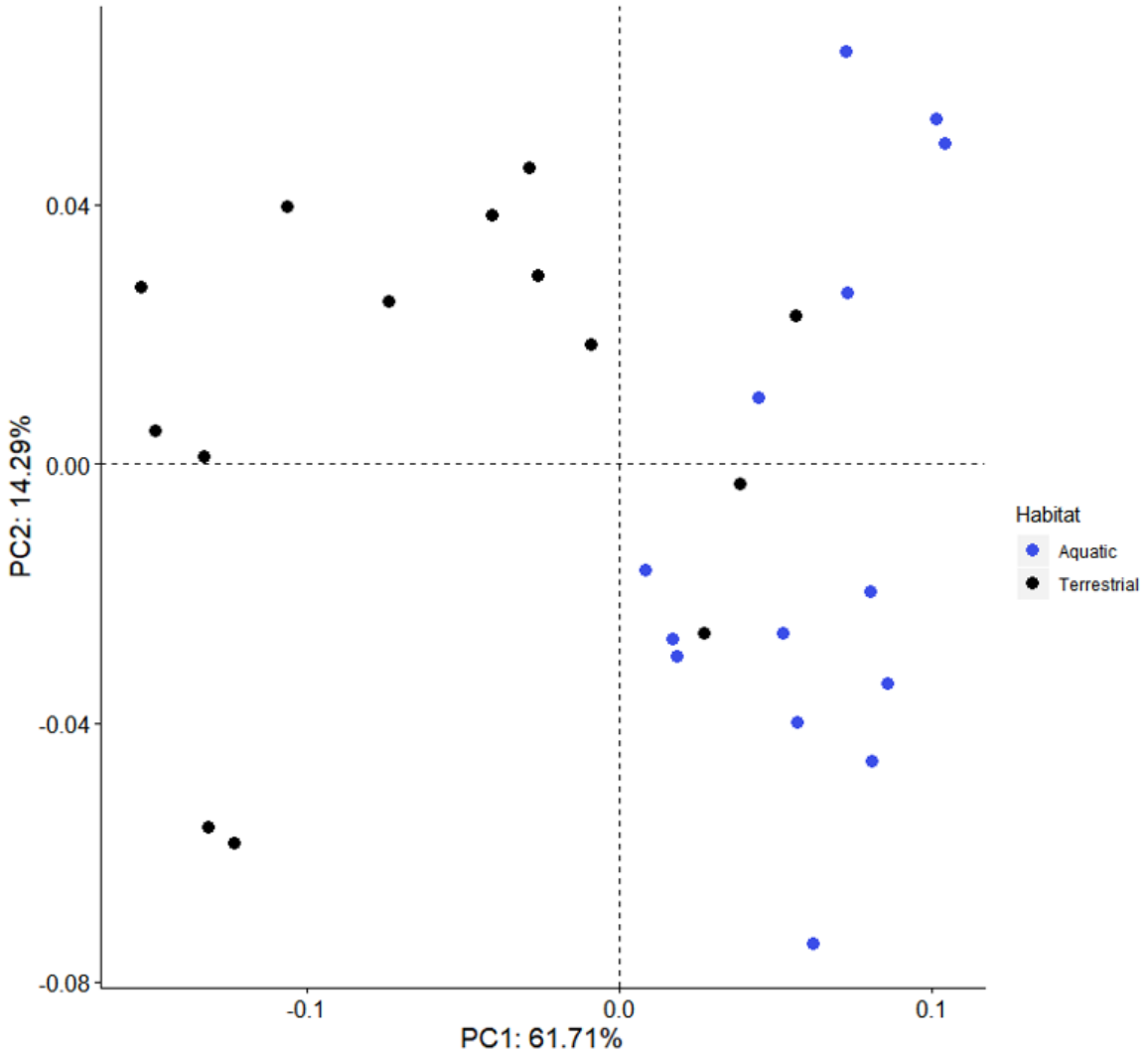

Figure 3.5. Morphospace resulting from a PCA using only data on *Ambystoma* crania. The first axis captures 61.71% of observed variation, and the second axis captures 14.29% of observed variation, with 76.0% of all variation represented by the first two principal component axes. Aquatic species tend to have higher PC1 values, though there is overlap in the space occupied by aquatic and terrestrial taxa.

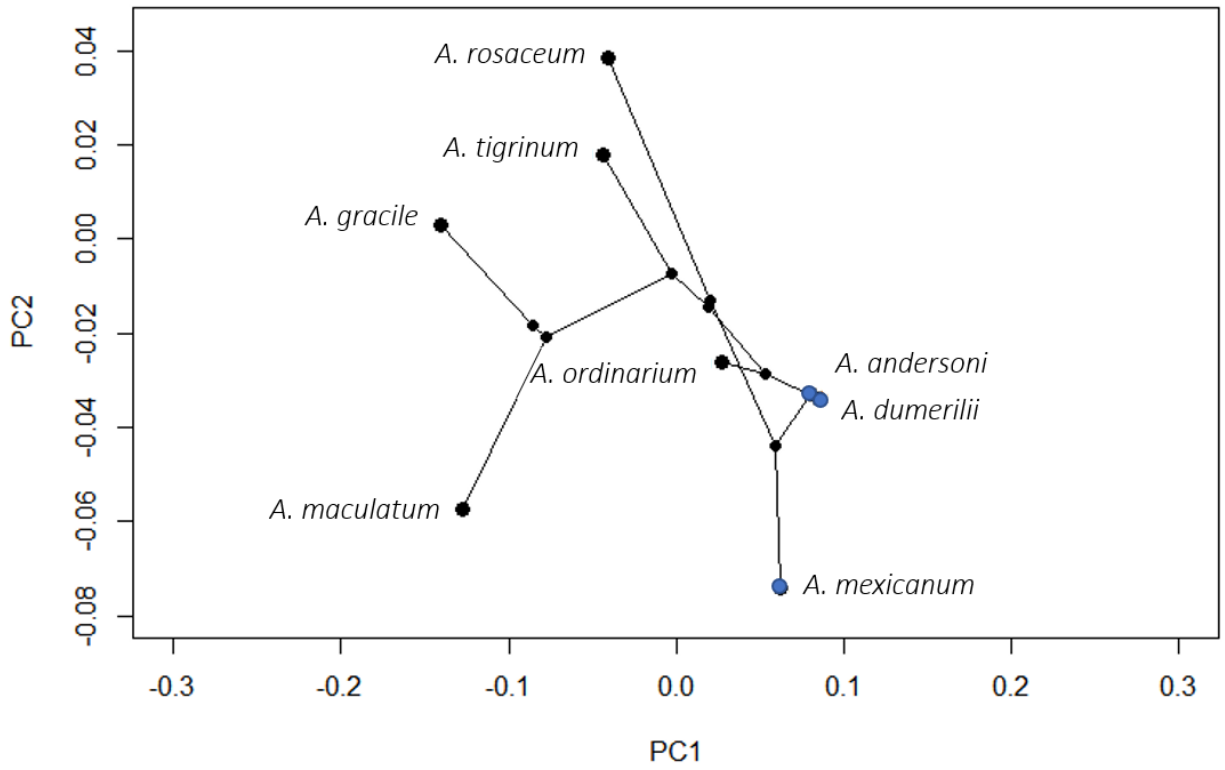

Figure 3.6. Phylomorphospace resulting from a PCA using only data on *Ambystoma* crania. Terrestrial species (in black) tend to have lower PC1 values than aquatic species (in blue) despite taxonomic closeness. Though there is overlap in the area occupied by aquatic and terrestrial species in Figure 3.5, superimposing a phylogeny shows that aquatic taxa are shifting towards more positive PC1 values relative to their terrestrial relatives, particularly between the sister taxa *A. andersoni* and *A. ordinarium*.

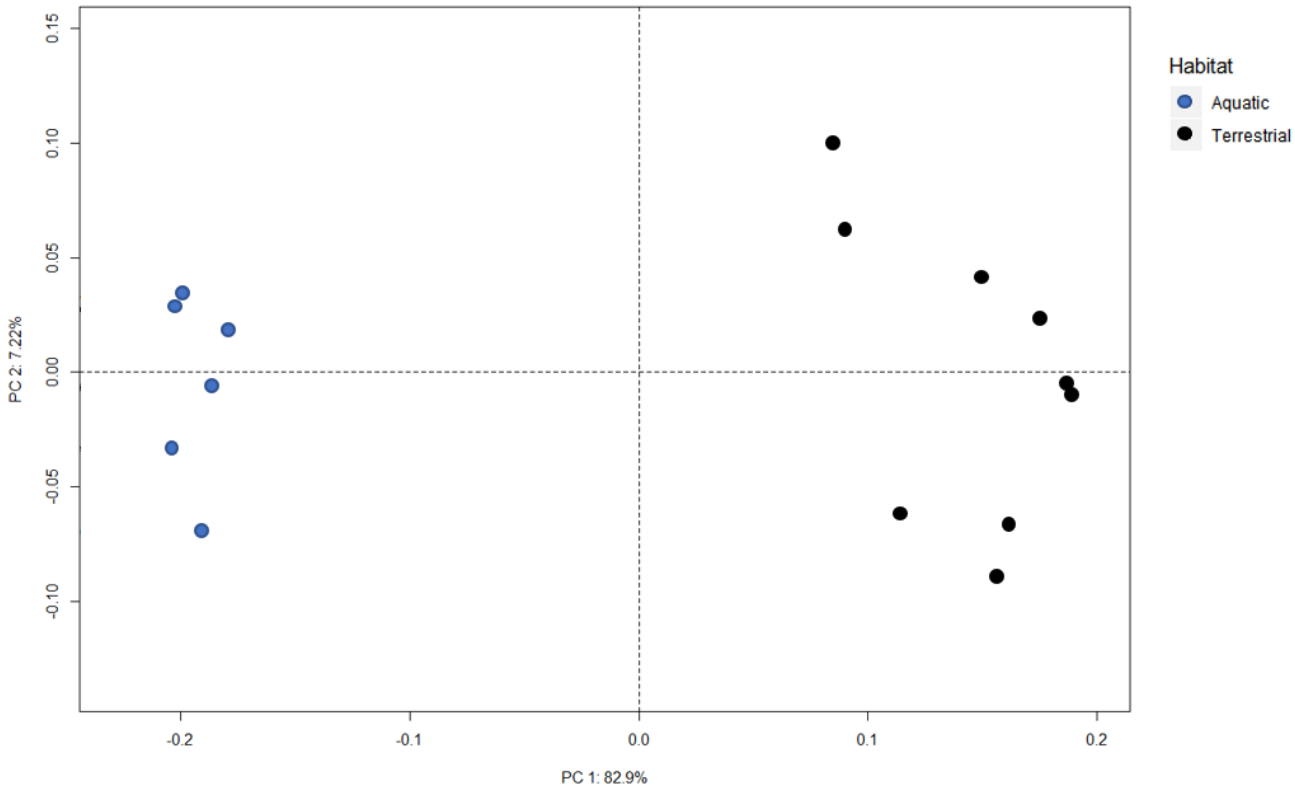

Figure 3.7. Morphospace resulting from a PCA using only data on Spelerpini crania. The first axis captures 82.9% of observed variation, and the second axis captures 7.22% of observed variation, with the first two axes combined capturing 90.12% of observed variation. The separation between habitats is more evident in Spelerpini than in *Ambystoma* (Figure 3.5).

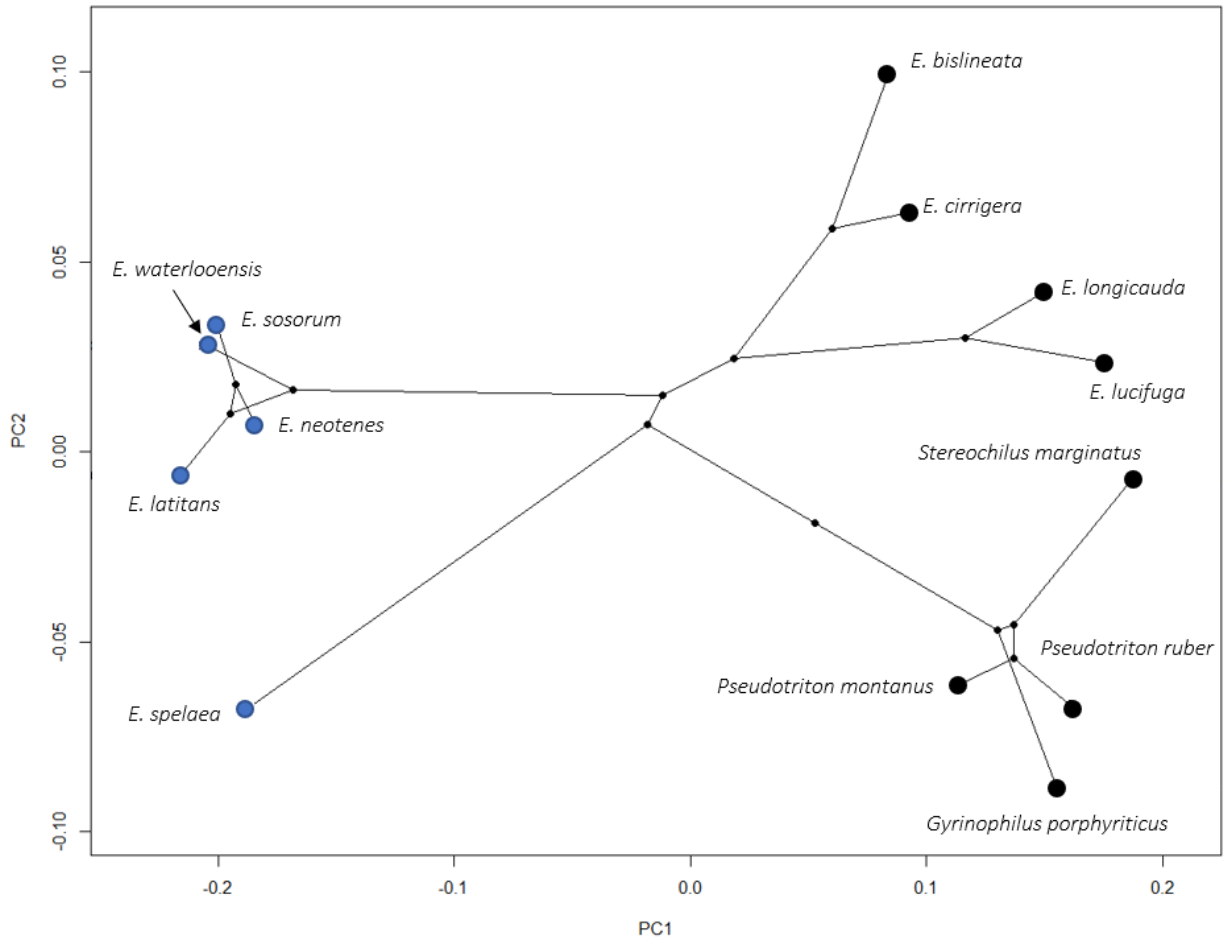

Figure 3.8. Phylomorphospace resulting from a PCA using only data on Spelerpini crania. Terrestrial species (in black) tend to have higher PC1 values than aquatic species (in blue). Superimposing the phylogeny shows how the terrestrial species of the *Eurycea* clade tend to have similar morphologies to the terrestrial species of the *Gyrinophilus* + *Pseudotriton* + *Stereochilus* clade.

Table 3.1. Observed habitat and metamorphic strategies in the *Ambystoma tigrinum* species complex. Adapted from Everson et al., 2021.

Species	Habitat	Metamorphic Strategy
A. altamirani	Streams, occasional ponds	Strong bias towards metamorphosis, neonates rare
A. amblycephalum	Ponds	Strong bias towards metamorphosis, neonates rare
A. andersoni	Lakes/ponds	Obligate neonate
A. bombypellum	Lakes/ponds, occasional streams	Strong bias towards metamorphosis, neonates rare
A. californiense	Vernal pools	Obligate metamorph
A. dumerilii	Lakes/ponds	Obligate neonate
A. flavipiperatum	Lakes/ponds, occasional streams	Both metamorphs and neonates commonly observed
A. granulosum	Lakes/ponds, occasional streams	Both metamorphs and neonates commonly observed
A. leorae	Streams	Strong bias towards metamorphosis, neonates rare
A. lermaense	Lakes/ponds	Both metamorphs and neonates commonly observed
A. mavortium	Lakes/ponds	Both metamorphs and neonates commonly observed
A. mexicanum	Lakes	Strong bias towards neonates, metamorphs rare
A. ordinarium	Streams	Both metamorphs and neonates commonly observed
A. rivulare	Streams	Strong bias towards metamorphosis, neonates rare
A. rosaceum	Streams	Both metamorphs and neonates commonly observed
A. silvense	Lakes/ponds	Both metamorphs and neonates commonly observed
A. taylori	Saline lake	Strong bias towards neonates, metamorphs rare
A. tigrinum	Lakes/ponds	Strong bias towards metamorphosis, neonates rare
A. velasci	Lakes/ponds, streams	Both metamorphs and neonates commonly observed

Table 3.2. Observed habitat and metamorphic strategies in spring salamanders. Salamanders inhabiting springs tend to live in surface waters such as streams and ponds, while subterranean species inhabit underwater caves and aquafer systems.

Species	Habitat	Metamorphic Strategy
Eurycea bislineata	Terrestrial	Terrestrial
Eurycea cirrigera	Terrestrial	Terrestrial
Eurycea latitans	Subterranean	Aquatic
Eurycea longicauda	Terrestrial	Terrestrial
Eurycea lucifuga	Terrestrial	Terrestrial
Eurycea neotenes	Springs	Aquatic
Eurycea quadridigitata	Terrestrial	Terrestrial
Eurycea sosorum	Springs	Aquatic
Eurycea spelaea	Subterranean	Aquatic
Eurycea waterlooensis	Subterranean	Aquatic
Gyrinophilus porphyriticus	Terrestrial	Terrestrial
Haideotriton wallacei	Subterranean	Aquatic
Pseudotriton montanus	Terrestrial	Terrestrial
Pseudotriton ruber	Terrestrial	Terrestrial
Stereochilus marginatus	Semiaquatic	Semiaquatic

Table 3.3. Description of the 3D landmarks used in the morphological analysis, which are all Type III Bookstein landmarks (Bookstein, 1997).

Landmark	Description
1	Anterior-most point on the rostrum, on the right premaxilla
2	The inflection point of the posterolateral curve of the right premaxilla
3	Anterior point of contact between the two vomer bones, from a palatal view
4	Posterior-most point of the right frontal
5	Most posterior ventral point where the two orbitosphenoids join, or the medial extent of the right orbitosphenoid if not joined
6	Most posterior dorsal point where the two orbitosphenoids join, or the medial extent of the right orbitosphenoid if not joined
7	Ventral-most point of the quadrate
8	Terminal point of the dentigerous process of the right maxilla

CHAPTER 4: MATERIAL PROPERTIES OF CRANIAL BONE IN THE MEXICAN AXOLOTL (*AMBYSTOMA MEXICANUM*)

Abstract

Salamanders have been used as modern analogs for biomechanical studies on the evolution of early tetrapods, However, without characterization of the material properties of their cranial bones, researchers use approximate values drawn from distantly related taxa, which can influence a model's fidelity. In this study, I performed nanoindentation tests on bone tissues from the crania of Mexican axolotls (*Ambystoma mexicanum*) to establish baseline values for Young's modulus that may be used in biomechanical models. I found average modulus values for three bones: the parasphenoid (3.8 GPa), left frontals (2.43 GPa), and right frontals (1.02 GPa). The parasphenoid showed the greatest range in values among all tests, suggesting that its involvement in prey capture and processing could have a strong influence on its stiffness due to bone remodeling or mineralization.

Introduction

The earliest tetrapods faced the challenge of co-opting structures that arose in aquatic ancestors for terrestrial life. Among those changes were feeding behavior, as suction feeding is ill-suited for land-feeding animals. Not only did their skulls change to reflect new feeding behaviors, but they had to retain the functions of protecting the central nervous system, housing sensory organs, and performing other tasks including burrowing. Modern salamanders present an interesting parallel with early tetrapods, as many have biphasic lifecycles and must transition from aquatic to terrestrial feeding. Additionally, unlike most tetrapods, the skulls of salamanders

have a significant cartilage component (Rose, 2003). Pliable material would appear ill-suited for the animal's mechanical demands, as salamanders use their heads for prey acquisition, intraspecific combat, and burrowing. Understanding the mechanical demands of a biphasic lifecycle may yield interesting conclusions about the utility of flexible support tissues as well as insight on the ancestral transition from water to land in the first tetrapods. However, these demands cannot be understood without a characterization of the underlying material properties of salamander bone. In this study, I characterized the salamander cranial bone by performing nanoindentation tests on samples from the Axolotl (*Ambystoma mexicanum*).

The mechanical properties of many biological materials are unknown (Currey 2010), and this has led to the adoption of perhaps ill-suited substitutions when making biomechanical models to test evolutionary or functional hypotheses. A large survey of materials is needed on a broader range of taxa and on structures with derivative functions such as the weaponized ribs in male ribbed newts (Heiss et al., 2010). Most experiments on bone material properties have been conducted on birds and mammals for their relevance to applied human medical research (Erickson, 1997). Erikson's (1997) survey of known biomechanical properties among amniotes highlighted this taxonomic sampling bias, as does Currey's (2010) call for work on poorly- or un-characterized mineralized structures. Young's modulus, the ratio of stress to strain and a proxy value for a material's stiffness, is one such property used in biomechanical modeling. At the time, known Young's modulus values determined through various experimental methods ranged from 6.65 GPa in crocodile skulls (Currey, 1987) and 9.0 GPa in *Anolis* lizard femora (Peterson and Zernicke, 1986) to 28.8 GPa in a *Phoenicopterus flamingo* tarsometatarsus (Currey, 1987).

Previous work concerning amphibian skull biomechanics have used different workarounds to perform comparative studies without access to precise material property values of anamniote skull bone. Zhou et al. (2017) compared a range of Young's modulus values (0.0665 GPa, 1.7 GPa, 3.35 GPa, 5.0 GPa and 6.65 GPa) in their work on Siberian salamander (*Salamandrella keyserlingii*) skulls; this range of values is comparable to the stiffness of rubber (0.01-0.1 GPa) to crocodile skull bone (6.65 GPa) (Engineering ToolBox, 2003). Kleinteich et al. (2012) built caecilian skull models using a modulus of 10 GPa, based on experiments on *Uromastyx* lizards (i.e., Moazen et al., 2008; Moazen et al., 2009). Most other amphibian skull biomechanical models, whether looking at extant Chinese Giant salamanders (*Andrias davidianus*) or Late Triassic temnospondyls, use a modulus of 6.65 GPa based on Currey's (1987) characterization of the frontal bone of *Crocodylus* (see Fortuney et al. 2015; Fortuny et al., 2016; Fortuny et al., 2017; Konietzko-Meier et al., 2018; Gruntmejer et al., 2019). Though biomechanical models may be used to compare relative performance of a structure when absolute values cannot be determined, as in the case of extinct animals (Rayfield, 2007), the quality of inputs is important, and the above substitutions may yield bad results if living amphibians have significantly different Young's modulus values.

The aim of this work is to provide the first characterization of stiffness in anamniote cranial bone. I examined Young's modulus of cranial bones in axolotl salamanders (*Ambystoma mexicanum*). These aquatic animals have lightly ossified skulls, even relative to terrestrial salamanders and other anamniotes, so the stiffness of their bones likely represents a minimum value among tetrapods. Nanoindentation was selected for testing based on its uniform methodology and reproducibility for other taxa and materials (Oliver and Pharr, 2004; Currey 2010).

Methods

Axolotl larvae were obtained from Backwater Reptiles, Inc., at approximately stage 55 of development (forelimbs were fully developed but only 3-4 posterior digits were visible to the naked eye), indicating larvae were 25 days post-hatching or older (Nye et al., 2003). They were maintained in accordance with approved husbandry procedures and fed a combination of frozen bloodworms and dried pellets (IACUC protocol 21012). Axolotls 1, 2, and 3 were sacrificed after 40 days ("Batch 1", >65 days post-hatching); axolotls 4, 5, and 6 were sacrifice after 76 days ("Batch 2", >101 days post-hatching) (IACUC protocol 21012).

Specimen Preparation

For nanoindentation testing, the frontal and parasphenoid bones were selected based on their relative flatness and lack of rugose surfaces. Right frontal bones were removed from the head of six euthanized axolotls (*Ambystoma mexicanum*) (IACUC Protocol # 21012). Bone dissection occurred immediately after euthanasia and decapitation. Initial dissection removed most of the muscle and connective tissue from the right side of the skull. The right frontal bone was then separated from the rest of the skull using a scalpel and fixed in 70% EtOH, following the safety protocols for biological materials at the University of Illinois Materials Research Laboratory. Following the dissection of the right frontal bone, the skulls were stored in 70% EtOH, with left frontal bones and parasphenoid bones dissected from the skull later.

Bones were cleaned of superficially visible carbon to expose the mineralized layer of bone by scraping the flat surface with a fresh scalpel. Thirty minutes prior to each test, the bones were mounted to a magnetic disk using superglue applied at two points so that the anterior and posterior ends of the bone were glued down and the medial portion of the bone was not saturated

with glue. Force was applied to the bone while glue dried to ensure a stable, flat surface. The sample was exposed to dry air during sample preparation and testing, with no measures taken to keep samples moist.

Nanoindentation of Axolotl Skull Bone

I examined nanomechanical properties of dry axolotl skull bone using nanoindentation performed on a Hysitron Triboindenter (Hysitron, Minneapolis, USA) with a light microscope mounted to the indenter to allow for precise control of sample position. A Berkovich tip was chosen due to its improved accuracy in measuring Young's modulus, at the expense of accuracy in measuring hardness (Kushch et al., 2007).

Tip-to-optics calibration was determined by nanoindentation of a sheet of aluminum. Seven indents were made, leaving clearly recognizable triangular marks in the shape of an H. Once properly calibrated, the cross hairs of the optical window aligned with the middle point of the H. The high number of calibration indents serves to both optically align the machine as well as clean any residue remaining on the tip from previous experiments, as the tip is shared by multiple researchers studying a variety of materials.

Indentation load functions were built following Ferrara et al. (2013): a trapezoidal load function with a 10 second linear loading segment, a 5 second hold period after the indenter reached a 1000 nanometer displacement, and a linear unloading segment of 10 seconds. The trapezoidal load function was selected as it has been shown to minimize the effect of creep in viscoelastic materials (Ebenstein & Pruitt, 2006; Oyen, 2013). The function held the indenter after it had penetrated 1000 nanometers of the sample, which resulted in maximum forces between 1037 μN and 1853 μN. Indents were performed towards the center of the sample on a

flat surface, as determined by the light microscope mounted on the indenter. Young's modulus and hardness were both recorded for the samples. Young's modulus for axolotl skull bone (E_b) was calculated from the experimental reduced elastic modulus (E_r) values using the equation:

$$\frac{1}{E_r} = \frac{1 - v_i^2}{E_i} + \frac{1 - v_b^2}{E_b}$$

The Berkovich diamond tip was assumed to have an elastic modulus (E_i) of 1141 GPa and a Poisson ratio (v_i) of 0.07 (Zysset et al., 1999; Ferrara et al., 2013). The Poisson's ratio for salamander bone (v_b) used in this calculation was 0.3 (Shahar et al., 2007). Results for the two bones tested were analyzed using one-way ANOVAs to compare the test means by individual and two-way ANOVAs by individual and batch using R (version 4.0.5).

Only successful tests are included; unsuccessful tests resulted from the inability to find a sufficiently flat surface on the microscale, causing the indenter tip to slide off the sample or contact the sample at an oblique angle. Improper contact with the sample is evident from the force-displacement curve produced: a smooth curve indicates proper contact, while deviation from the typical smooth curve shape indicates improper contact. Neither frontal bone from axolotl 6 resulted in a successful test, nor did the parasphenoid from axolotl 1.

Results

The results of nanoindentation tests on the left and/or right frontal bones of axolotls 1-5 are reported in Table 4.2, and the results of tests on the parasphenoid are reported in Table 4.3. Figure 1 plots the range of data from all tests according to the type of bone tested. The parasphenoid results had the greatest range in values (0.54 GPa – 13.34 GPa). All parasphenoid

tests averaged to a value of 3.88 GPa. All tests of the left frontal averaged to a value of 2.43 GPa, and all tests of the right frontal averaged to 1.02 GPa. A plot of all test results according to the date of the nanoindentation test is given in Figure 4.2. The test values show only a weak correlation with the time between the beginning of the study and the test date (R^2 =0.205).

A one-way ANOVA on all the test results for both left and right frontal bones categorized by individual showed differences between individuals (P-value of 0.04) (Table 4.4). A 2-way ANOVA that also included batch as a category found differences both among individuals and between the two batches (P-values of 0.019 and 0.005, respectively) (Table 4.5). While both a one-way ANOVA (Table 4.6) and two-way ANOVA (Table 4.7) on the presphenoid test results do not support significant differences among individuals (P-values of 0.38 and 0.32, respectively), the two-way ANOVA did find differences between the two batches (P-value of 0.004).

Discussion

The averages Young's modulus of all bones tested were lower than the 6.65 GPa value commonly used for biomechanical models of salamander skull bone. A greater range of modulus values were observed in parasphenoid bones, which were tested over two months after the frontal bones. This may be due to the effect of ethanol fixative on the soft tissues or cellular structure, though this is only weakly supported by the linear regression shown in Figure 4.2. Specimen preparation can change modulus values: for example, Currey et al. (2008) found that rehydrated long bone in red deer (Cervus elaphus) had a 7% lower Young's Modulus than dry long bone.

Though the parasphenoid test results show a greater range in values, it was easier to perform nanoindentation tests on this bone due to its flatness and smoothness (lacking the rugose muscle attachments sometimes observed on the axolotl frontal bones), as well as its size which

facilitated stable mounting of the bone to the magnetic wafer. All but one parasphenoid bone dissected from the 6 axolotls did not result in any successful tests, and more tests were successful thus resulting in a larger number of data points. Surface roughness has been shown to increase material property variability in nanomechanical testing (Donnelly et al., 2006). Future work should use a polishing pretreatment of bone to standardize the effects of surface roughness to reduce the number of unsuccessful tests due to oblique contact between the indenter tip and the sample. Additionally, polishing would serve to standardize the thickness of the samples, which was not standardized in this study.

Differences between the mean modulus values of parasphenoid and frontal bone may result from functional demands. The parasphenoid may be thought of as a brace between the anterior, tooth-bearing elements and the posterior braincase, and may need to be stiffer than the frontal bone. Also, the parasphenoid comes into direct contact with food items, unlike the frontal bone, and Axolotls raised for this study were fed a diet of ≥50% hard pellets that the animals manipulated in their buccal cavity between suction feeding and swallowing. Behavioral differences among individuals meant some were ingesting pellets immediately after they were introduced to the tank, while other individuals did not notice pellets until after they had become waterlogged and somewhat softer. Different food hardness could have led to differing remodeling and mineralization in the skull, primarily in bones involved in feeding. Future work should record individual behavioral peculiarities and make attempts to standardize the hardness of introduced food.

The average Young's modulus for the cranial bones of axolotls are lower than the modulus of *Crocodylus* frontal bone (6.65 GPa) used in modeling extant and extinct amphibian skull biomechanics, with some individuals having modulus values nearly an order of magnitude

smaller. E_b is also lower than most of the estimated moduli used by Zhou et al. (2017) in analyzing cranial biomechanics of adult *Salamandrella keyserlingii*. In their study of the median fontanelle region of *S. keyserlingii*, they found that adding tissue to this otherwise empty region on the dorsal side of the skull did not significantly change stresses experienced by the skull during two prey prehension loads when that tissue had a Young's modulus of 1.7 GPa or lower. At higher modulus values, the added tissue helped dissipate stress. They argue that this is evidence for biomechanical optimization through reduction of developmental costs. The average modulus values observed in this study for left and right frontals (2.43 GPa and 1.02 GPa) are near to their study's 1.7 GPa value. That Zhou et al. noted functional differences between low modulus values and the 6.65 GPa standard in the literature implies that this magnitude of change is potentially sufficient to produce significantly different results in biomechanical modeling, and that greater caution should be taken in building models of extinct anamniotes.

Conclusion

This study is the first to characterize the Young's modulus of anamniote cranial bone. It demonstrates that realistic values for salamander bone may be as low as 1 GPa, though there is likely great variation within individuals due to functional demands and degrees of mineralization. It remains to be seen if terrestrial salamanders have stiffer bones due to greater mineralization, as well as what effect prey hardness has on bone remodeling. Nonetheless, given the lower values observed in this study relative to the standard use of 6.65 GPa for salamander skull bones, future work should take lower values into consideration in modeling the biomechanical performance and evolution of amphibian skulls.

Figures and Tables

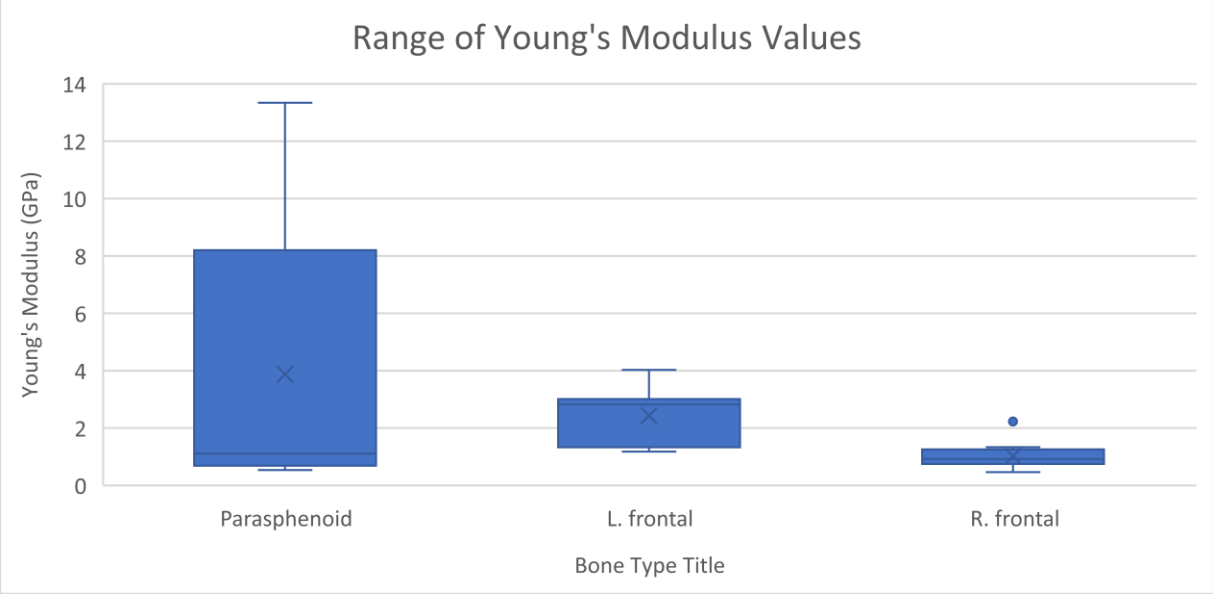

Figure 4.1. The range of Young's modulus values (GPa) for different cranial bones in the axolotl obtained by nanoindentation. The averages for all samples, by bone, were: parasphenoid, 3.88 GPa; left frontal, 2.43 GPa; right frontal, 1.02 GPa.

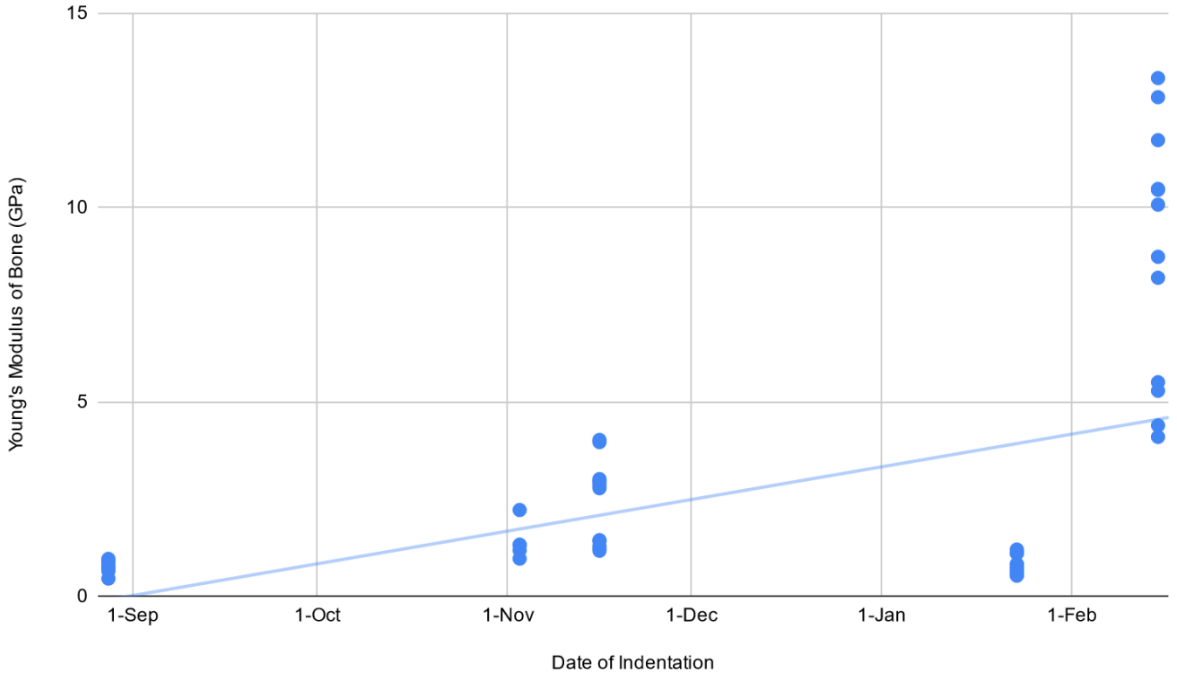

Figure 4.2. The Young's modulus values (GPa) by date indentations were performed. All axolotl tissues were fixed in ethanol within a short period of time, with nanoindentation tests performed at later dates. Tests performed later (>5 months after fixing) had higher Young's modulus values. A linear regression of all data points yields a line with a positive slope with an R^2 value of 0.205.

Table 4.1. Snout-to-vent measurements, approximate age at sacrifice, and "batch" for each axolotl.

Individual	SVL (cm)	Batch	Approximate Age Post-hatching
1	4.8 cm	1	>65 days
2	4.6 cm	1	>65 days
3	5.1 cm	1	>65 days
4	5.0 cm	2	>101 days
5	4.9 cm	2	>101 days
6	4.7 cm	2	>101 days

Table 4.2. Experimental data for reduced elastic modulus (E_r) and calculated Young's modulus (E_b) for axolotl frontal bone. E_b was calculated using Equation 1 assuming a Poisson ratio for bone of 0.3.

Individual	Structure	Reduced Elastic Modulus (E_r) (GPa)	Calculated Young's Modulus (E_b) (GPa), vb=0.3	E_b range (GPa) for v_b=0.2 to v_b=0.35
1	R. frontal	0.72307	0.66	0.64-0.70
1	R. frontal	0.80238	0.73	0.71-0.77
1	R. frontal	0.88914	0.81	0.78-0.86
Average			**0.74**	
2	L. frontal	3.23	2.98	2.88-3.15
2	L. frontal	1.58	1.45	1.40-1.53
2	L. frontal	1.35	1.24	1.19-1.30
2	L. frontal	1.29	1.18	1.14-1.25
2	L. frontal	1.55	1.42	1.37-1.50
2	L. frontal	1.42	1.30	1.25-1.37
Average		`	**1.59**	
3	R. frontal	0.98512	0.90	0.87-0.95
3	R. frontal	0.50947	0.46	0.45-0.49
3	R. frontal	1.06	0.97	0.93-1.0
3	R. frontal	1.01	0.92	0.89-0.97
3	R. frontal	0.8381	0.77	0.74-0.81
Average			**0.80**	
4	R. frontal	1.3	1.19	1.15-1.26
4	R. frontal	1.45	1.33	1.28-1.40
4	L. frontal	4.34	4.03	3.88-4.25
4	L. frontal	3.1	2.86	2.76-3.02
4	L. frontal	3.2	2.95	2.85-3.12
4	L. frontal	4.28	3.97	3.83-4.19
4	L. frontal	3.18	2.94	2.83-3.10
4	L. frontal	3.27	3.02	2.91-3.19
Average			**2.79**	
5	R. frontal	1.07	0.98	0.94-1.01
5	R. frontal	1.46	1.34	1.29-1.41
5	R. frontal	2.42	2.23	2.15-2.35
Average			**1.51**	

Table 4.3. Experimental data for reduced elastic modulus (E_r) and calculated Young's modulus (E_b) for axolotl parasphenoid bone. E_b was calculated using Equation 1 assuming a Poisson ratio for bone of 0.3.

Individual	Structure	Reduced Elastic Modulus (E_r) (GPa)	Calculated Young's Modulus (E_b) (GPa), v_b=0.3	E_b range (GPa) for v_b=0.2 to v_b=0.35
2	Parasphenoid	0.694022	0.633525392	0.61-0.668
2	Parasphenoid	0.609258	0.555938814	0.53-0.586
2	Parasphenoid	0.68147	0.622032517	0.59-0.656
2	Parasphenoid	0.589596	0.537950124	0.51-0.567
2	Parasphenoid	0.61521	0.561384902	0.54-0.592
2	Parasphenoid	0.744648	0.679892755	0.65-0.717
Average			**0.598454084**	
3	Parasphenoid	10.555204	10.08086879	9.72-10.63
3	Parasphenoid	12.196154	11.73844256	11.3-12.38
3	Parasphenoid	10.956322	10.48368917	10.1-11.05
3	Parasphenoid	10.933789	10.46102028	10.0-11.03
3	Parasphenoid	13.754201	13.33625278	12.8-14.06
3	Parasphenoid	13.27603	12.84336189	12.3-13.54
Average			**11.49060591**	
4	Parasphenoid	0.658661	0.601151429	0.57-0.634
4	Parasphenoid	0.752163	0.686777391	0.66-0.724
4	Parasphenoid	0.82663	0.755023138	0.72-0.796
4	Parasphenoid	1.212868	1.109726283	1.07-1.170
4	Parasphenoid	1.322958	1.211053493	1.16-1.277
4	Parasphenoid	1.242504	1.136993494	1.09-1.199
4	Parasphenoid	1.225032	1.120917142	1.08-1.182
Average			**0.94594891**	
5	Parasphenoid	9.208152	8.739124526	8.42-9.219
5	Parasphenoid	4.424826	4.107840524	3.96-4.333
5	Parasphenoid	5.670939	5.294772185	5.10-5.585
5	Parasphenoid	4.735498	4.402493741	4.24-4.644
5	Parasphenoid	5.898927	5.513402079	5.31-5.816
5	Parasphenoid	8.662046	8.199958903	7.90-8.650
Average			**6.042931993**	
6	Parasphenoid	0.820883	0.74975464	0.72-0.790
6	Parasphenoid	0.878447	0.802538063	0.77-0.846
6	Parasphenoid	0.91602	0.83700541	0.80-0.882
6	Parasphenoid	0.903695	0.82569787	0.79-0.871
6	Parasphenoid	0.791403	0.722733451	0.69-0.762
6	Parasphenoid	0.91009	0.831564791	0.80-0.877
Average			**0.794882371**	

Table 4.4. ANOVA table for all frontal bone test results, by individual.

Source of Variation	Sum of Squares	*df*	Mean Squares	*F*-ratio	*P*
Individual	4.5017	1	4.5017	4.6873	0.04055
Error	23.0498	24	0.9604		
Total	27.5515	25			

Table 4.5. 2-Way ANOVA table for all frontal bone test results, by individual and batch.

Source of Variation	Sum of Squares	*df*	Mean Squares	*F*-ratio	*P*
Individual	4.502	1	4.502	6.355	0.01909
Batch	6.758	1	6.758	9.540	0.00518
Residuals	16.292	23	0.708		

Table 4.6. ANOVA table for all parasphenoid test results, by individual.

Source of Variation	Sum of Squares	*df*	Mean Squares	*F*-ratio	*P*
Individual	15.33	1	15.331	0.7783	0.3849
Error	571.22	29	19.697		
Total	586.55	30			

Table 4.7. 2-Way ANOVA table for all parasphenoid test results, categorized by individual and batch.

Source of Variation	Sum of Squares	*df*	Mean Squares	*F*-ratio	*P*
Individual	15.3	1	15.33	1.010	0.32344
Batch	146.3	1	146.33	9.643	0.00432
Residuals	424.9	28	15.17		

CHAPTER 5: FUNCTIONAL PERFORMANCE OF THE LOWER JAW VARIES ACCORDING TO HABITAT TYPE IN TWO SALAMANDER FAMILIES

Abstract

Feeding is one of the biggest evolutionary challenges faced by organisms that transition between habitats, such as early tetrapods that co-opted structures suitable for aquatic environments for life on land. The study of secondarily aquatic species may shed light on the mechanics of these significant habitat shifts. I compared the jaw morphology of two salamander groups that contain both aquatic and terrestrial salamanders: mole salamanders (Ambystomatidae) and spring salamanders (Plethodontidae, tribe Spelerpini). A finite element analysis was also conducted to compare shape and material stiffness in a simulated bite to see if terrestrial species are better able to perform jaw prehension for prey capture. I found differences in the length-to-width ratio of the mandible between aquatic and terrestrial taxa in the whole data set and within the well-sampled *Ambystoma*. However, the biomechanical analysis produced conflicting results, where stiffer materials produced models with lower maximum effective stresses, but the terrestrial morphology had higher maximum effective stress values than the aquatic morphology analyzed. This may suggest that bite force is not a strong selective force on jaw morphology in salamanders, which are generalist carnivores that mainly feed with tongue prehension.

Introduction

The earliest tetrapods faced the challenge of co-opting structures that arose in aquatic ancestors for terrestrial life. Among those changes were feeding behavior, as suction feeding is

ill-suited for land-feeding animals. Not only did their skulls change to reflect new feeding behaviors, but they must also retain the functions of protecting the central nervous system, housing sensory organs, and performing other tasks including burrowing. Modern salamanders present an interesting parallel with early tetrapods, as many have biphasic lifecycles and must transition from aquatic to terrestrial feeding. Understanding the mechanical demands of a biphasic lifecycle may yield interesting conclusions about the ancestral transition from water to land in the first tetrapods.

Moving from aquatic to terrestrial feeding generally means shifting from suction feeding to either tongue protraction or jaw capture. All terrestrial species use tongue protraction, though jaw capture is also used in certain groups (Wake and Deban, 2000). Typically prey items are small enough to be brought fully into the oral cavity. However, biting is necessary for immobilizing large prey and has a role in intraspecific aggression (Wake and Deban, 2000). Jaw capture is unusual but has been observed in Ambystomatidae, Salamandridae, and Plethodontidae, particularly when the tongue fails to apprehend the prey (Larsen and Guthrie, 1975; Miller and Larsen, 1990; Wake and Deban, 2000). Wake and Deban (2000) note that quantitative kinematic studies are limited in taxonomic scope, conducted under artificial conditions, and occasionally use unnatural prey, while behavior modulation is described in only a couple species despite the diversity of prey types observed in most species. There is little available data on bite force as well. Deban and Richardson (2017) found that *Pseudotriton ruber* achieved an average peak bite force of 0.64±0.20 N, while *Desmognathus quadramaculatus*, which has particularly well-ossified jaws and unusual atlanto-mandibular ligaments for amplifying force, had an average peak bite force of 8.2±1.3 N, with one bite recorded at 14.3 N. The larger bite forces may facilitate *D. quadramaculatus* to feed on other lungless salamanders,

while most other genera are generalist carnivores that eat primarily invertebrates and likely have bite strengths similar to those of *P. ruber*.

Differences in the cranial morphology between aquatic and terrestrial species have been demonstrated irrespective of diet (Chapter 3). While the cranium is under selection for multiple functions (feeding, burrowing, sensory structures, and protecting the braincase), the lower jaw of salamanders is primarily used in feeding. I hypothesize here that mandible morphology differs between aquatic and terrestrial taxa, and that these differences will correspond to greater ability to withstand bite forces. I also tested if stiffer materials, such as those in terrestrial animals with greater bone mineralization, are better suited for withstanding bite forces. To test these hypotheses, I examined mandibles from two salamander families: mole salamanders (Ambystomatidae) and spring salamanders (Plethodontidae, tribe Spelerpini). Both families have secondarily aquatic species, presenting the opportunity to compare the habitat shift in two independent cases.

Methods

Linear measurements of the jaw

Sixty-two individuals representing 28 taxa were included in the study. Three-dimensional shape data was collected from microCT scans of museum specimens from the Field Museum of Natural History and the Illinois Natural History Museum; these were scanned at the Imaging Technology Group of the Beckman Institute for Advanced Science and Technology. The remaining dataset was drawn from the online repositories Morphosource.org and Phenome10k.org. Raw scan data was sectioned using Avizo (ThermoFischer Scientific) and exported as .stl files.

Overall length and width of jaws was measured three times per individual (Figure 5.1), with the average length for each measure used to calculate a length:width (LW) ratio. When there were multiple individuals per species in the dataset, a species average was calculated from all length:width ratios. Measurements were taken using the linear measuring tool in Blender (version 3.4.1). The relationship between habitat (aquatic vs. terrestrial) or genus and LW ratio was analyzed using one-way ANOVA using R (version 4.0.5). An additional one-way ANOVA was conducted for *Ambystoma* specimens, as this genus was the best represented in this dataset (N=21).

Biomechanical performance of the jaw

Sample and digitization – Two Spelerpini species were analyzed: the terrestrial *Gyrinophilus porphyriticus* (teaching collection, UIUC School of Integrative Biology) and the aquatic *Eurycea* (*Haideotriton*) *wallacei* (FMNH 109962). Plethodontid salamanders were chosen as some bite forces for this family have been reported (Deban and Richardson, 2017), and the bite force of *G. porphyriticus* should be comparable to that of the closely related *Pseudotriton ruber*. Whole skulls were CT scanned at the Imaging Technology Group of the Beckman Institute for Advanced Science and Technology at the University of Illinois. CT scan data were imported to the software Avizo (version 9.5.0, FEI-VSG Company), where the models were reconstructed and segmented to create a stl shapefile of only the jaw bones. Shapefiles were made manifold and scaled to the same total volume in Blender (version 3.4.1), then were decimated and smoothed using Geomagic Wrap 2017 (3D Systems) before being exported as. iges surface files. Though the mandible consists of multiple bones, sutures were ignored for the purposes of this analysis and the entire mandible was treated as a single structure.

Model properties – A structural mechanics analysis was used to evaluate the biomechanical behavior of the jaw in FEBio Studio (version 1.3.0). The mechanical properties of the bone were varied based on initial results reported in Chapter 4 (which ranged from approximately 0.5 - 11.5 GPa), as no other properties for anamniote skull bone have been published. This analysis varied the stiffness of the jaw bone to test the impact of stiffness on bite mechanics using the following inputs: 0.5 GPa, 1 GPa, 5 GPa, 10 GPa, and 15 GPa (from low to high stiffness). Elastic, linear, isotropic material properties and a bone density of $1 g/cm^3$ were assumed. The analysis used a Poisson's ratio of 0.3 (Shahar et al., 2007). Though some of the mechanical conditions of this test may not be biologically relevant, a controlled comparative analysis has been demonstrated to be useful for biological questions (Rayfield, 2007; Strait et al, 2005; Gi et al., 2015), and sensitivity analyses suggest results for modeled heterogeneous bone closely match those for modeled homogeneous bone (Walmsely et al., 2013).

Boundary and loading conditions – Boundary conditions were defined as the muscle insertion sites for the mm. levatores mandibulae on both supraangulars, which was pinned for no allowed displacement or rotation. A nodal force was applied to the dorsal surface of the anterior portion of the jaw, above the symphysis, where the tooth row sits. This force simulated a bite, and a force of 0.5 N was used based on the average peak bite force for *P. ruber* of 0.64±0.20 N found by Deban and Richardson (2017). A second set of analyses were conducted on *H. wallacei* mandibles with given Young's moduli of 0.5 and 15 GPa and an applied force of 10 N to simulate large bite forces like those achieved by *D. quadramaculatus*.

Results

Linear measurements of the jaw

Statistically significant ($p \leq 0.05$) differences were found for the mean LW ratio in species from different habitats (Table 5.1, Figure 2B) and genera (Table 5.2, Figure 2A). Habitat also influences LW ratio in *Ambystoma* (Table 5.3, Figure 2C). Aquatic species tend to have relatively shorter and wider jaws than terrestrial species, which have relatively longer and narrower jaws.

Biomechanical performance of the jaw

The distribution and values of effective stresses were recorded for different given material property values in two species simulating a 0.5 N bite force. Two additional analyses used a 10 N bite force in an *E. wallacei* jaw with modulus values of 5 GPa and 15 GPa. Localized areas of high stress are to be expected near the edge of boundary conditions, given the geometric structure of the mesh. These are typically excluded as outliers when analyzing FEA results. For this reason, resulting graphical representations are scaled to eliminate obvious outliers and facilitate visual comparisons. However, maximum observed values for effective stress are given in Table 5.4.

The general pattern of stress on the mandibles were similar among all tests, with an area of high stress at the symphysis where the force was applied and a region of artificially elevated values at the anterior extent of the boundary condition. The ventral edge of the mandible had relatively lower stresses spread out over a large area, while the dorsal edge had more concentrated areas of higher stress. The dorsal edge corresponds to the dentary, the tooth-bearing bone on the mandible and the one that comes in direct contact with prey items. While the

effective stresses experienced in the high-force analysis were a magnitude of order higher, the overall patterns of effective stress were similar to the low-force results (Figure 5.4).

Discussion

Overall jaw morphology varied between aquatic and terrestrial species in both families. However, this did not translate to differences in the stress patterns in the biomechanical model. The maximum effective stress was higher in the terrestrial species, but as these values are outliers created by inherent effects of a pinned boundary condition on the mesh, the distribution of stresses in the rest of the mandible require further quantification. However, maximum effective stress was negatively correlated with stiffness, such that the models with lower Young's modulus values had higher maximum effective stresses. Higher values in the terrestrial species but lower values in stiffer materials do not support the initial hypothesis that terrestrial species in general can withstand bite forces better than aquatic species. One potential confounding factor may have been the larger muscle attachment surface of the aquatic species, and therefore the size of the pinned boundary condition. Future studies may eliminate this source of error by creating an artificial geometry approximating mandible shape in living a taxon then selectively making it wider or narrower while keeping the muscle attachment site the same size.

It is possible that the overall mandible morphology is not the limiting factor in producing bite force. For example, in the case of *Desmognathus quadramaculatus*, increased bite force is achieved by modified joints, stronger muscles, and unusual ligaments that are more efficient at generating forces (Deban and Richardson, 2017). The observed difference in jaw shape between the two habitats in both families may be driven by one, or both, of the following factors: ontogenetic development, or suction feeding mechanics. Wider mandibles could facilitate faster

or more forceful suction feeding due to its influence on buccal cavity shape. These hypotheses could be tested in true salamanders and newts (family Salamandridae). This family includes groups such as the Pacific newts (*Taricha spp.*) which are fully terrestrial in adulthood, which may be compared to the triphasic newts that have a post-metamorphic, terrestrial 'eft' phase but become aquatic at sexual maturity.

The morphology and function of the mandible should not be considered in isolation when considering all the behaviors it is involved in. There may be skull-jaw interactions that would confound an analysis of the jaws or the cranium in isolation. For example, the jaw may brace the cranium during head-first burrowing. Many terrestrial salamanders burrow to escape predators or maintain skin moisture, and a mandible bracing against the cranium may need to withstand stronger compressive forces along its long axis. Also, while this study examined forces applied during a single bite, a more biologically relevant scenario would be successive bites spanning prey capture, processing, and ingestion. Resistance to torsion may be a more relevant functional performance metric while the salamander attempts to subdue moving prey. Rull et al. (2020) suggested that axolotls may modulate bite speed, force applied, and gape cycles based on different prey items, possibly due to perceived cues for prey evasiveness or hardness. A comprehensive study on the functional performance of the mandible should include considerations for successive loading consistent with observed gape cycles in living salamanders.

Within the larger context of the evolution of tetrapods, shifting to terrestrial habitats may have led to a release of constraints on the lower jaw morphology as they did not need to generate the large forces needed for suction feeding. This is consistent with the findings of Anderson et al. (2013) that functional variation in tetrapod mandibles did not experience an increased rate of evolution as they became more terrestrial, in contrast to rapidly changing postcranial features. Still,

other applications of force on the mandible, such as torsion while subduing prey or compression while bracing the skull during burrowing, should be considered in examining fossil taxa.

Conclusion

The jaw morphology in both families studied shows similar patterns: aquatic species have relatively shorter and wider mandibles than terrestrial species. This holds true both within the genus *Ambystoma* and in the larger dataset including mole and spring salamanders. However, finite element analyses on the mandible in a terrestrial and aquatic spring salamander failed to support the hypothesis that terrestrial jaw morphologies can better withstand the forces associated with jaw prehension feeding. Jaw morphology may be influenced by other factors, such as selective pressure on shape for suction feeding in aquatic taxa, or it may be a by-product of ontogeny. Togue-prehension feeding in terrestrial salamanders may release lower jaws from selective pressures in all but the most specialized taxa.

Figures and Tables

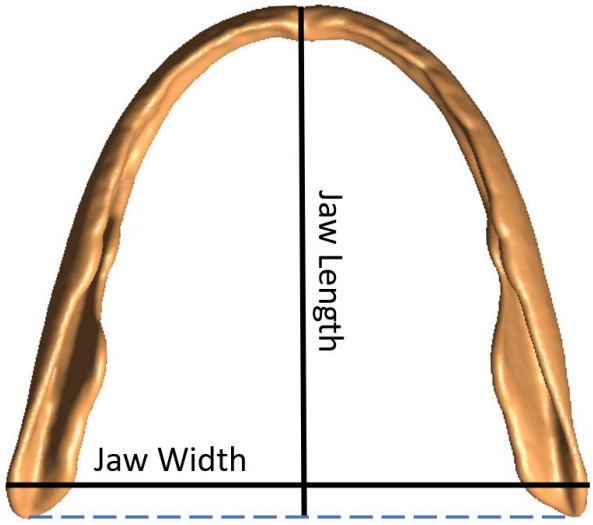

Figure 5.1: Linear measurements (solid lines) captured for analysis. Jaw length was measured from the anterior point of the jaw symphysis to the posterior extent of the mandible (blue dashed line). A length-to-width ratio was calculated using these linear measurements to compare general mandible proportions within the dataset. Measurements are shown on a modified 3-D model of a *Eurycea wallacei* mandible, shown in dorsal view.

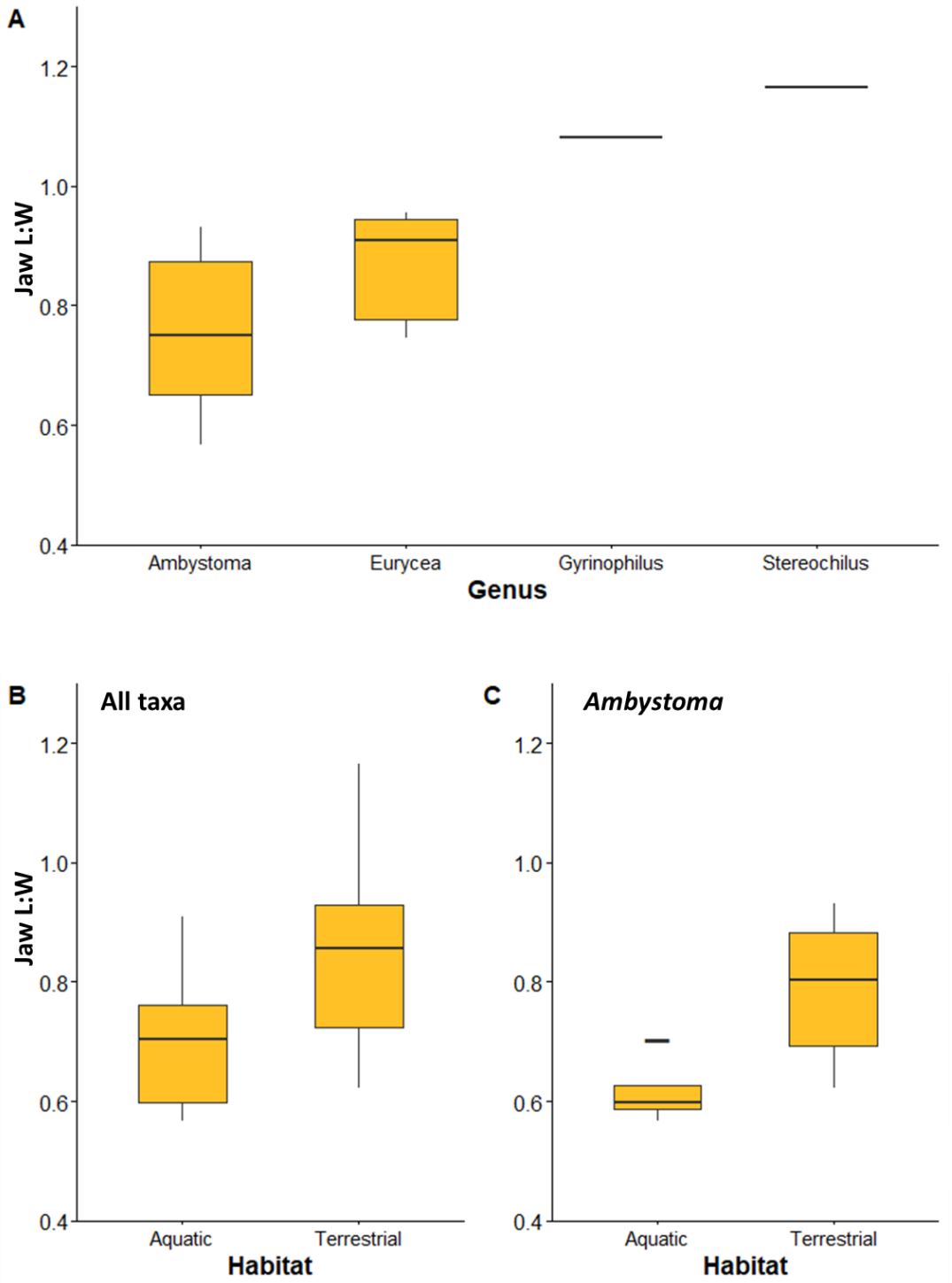

Figure 5.2: Sixty-two specimens were measured representing 28 species. The average jaw length:width radio was taken for each species. Box plots show the average and range for the length:width ratio among ambystomatid and Spelerpini plethodontid salamanders by genus (A, top) and habitat (B, bottom left). Most species in the study are in the genus *Ambystoma* (n = 21), and results for only *Ambystoma* are presented separately (C, bottom right).

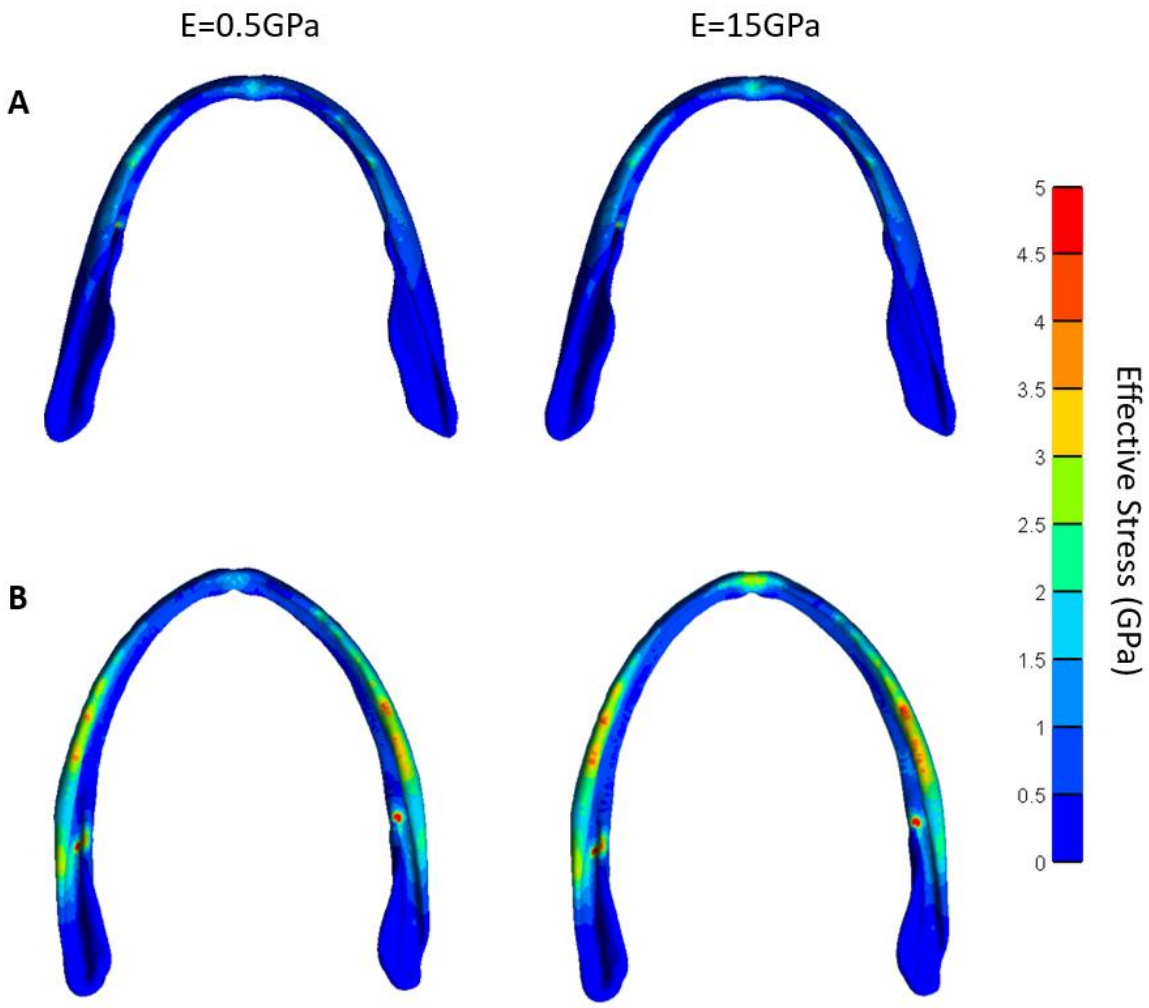

Figure 5.3. Effective stress results (in GPa) of anterior biting with a force of 0.5 N, comparable with *Pseudotriton ruber* bite forces, in the mandible of *Eurycea wallacei* (**A**) and *Gyrinophilus porphyriticus* (**B**), shown in dorsal view, with Young's modulus values (E) of 0.5 GPa (left) and 15 GPa (right). The scale for effective stress was capped at 5 GPa to assist in visualizing results.

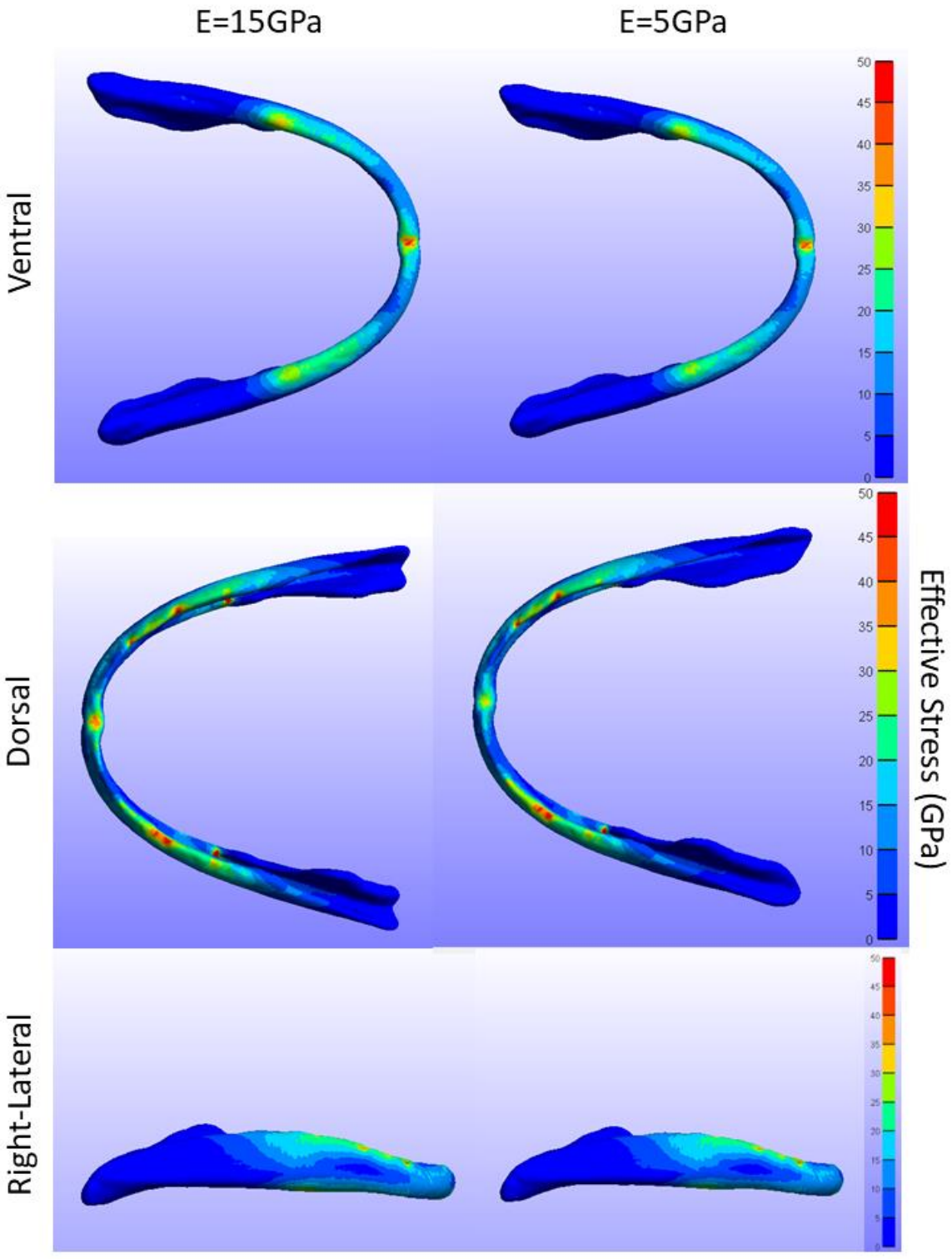

Figure 5.4. Effective stress results (in GPa) of anterior biting with a force of 10N, comparable with *Desmognathus spp*. bite forces, in the mandible of *Eurycea wallacei* with a Young's Modulus value of 15 GPa (left) and 5 GPa (right). Results are presented in ventral (top), dorsal (middle) and right-lateral (bottom) views. The scale for effective stress was capped at 50 GPa to assist in visualizing results.

Table 5.1: One-way ANOVA on LW ratio and habitat of all species (aquatic vs terrestrial)

Source of Variation	Sum of Squares	*df*	Mean Squares	*F*-ratio	*P*
Habitat	0.09661	1	0.096608	4.9308	0.03531
Residuals	0.50941	26	0.019593		
Total	0.60582	27			

Table 5.2: One-way ANOVA on LW ratio and genus of all species

Source of Variation	Sum of Squares	*df*	Mean Squares	*F*-ratio	*P*
Genus	0.27634	3	0.092114	6.7059	0.001908
Residuals	0.32967	24	0.013736		
Total	0.60601	27			

Table 5.3: One-way ANOVA on LW ratio and habitat, for *Ambystoma* data only

Source of Variation	Sum of Squares	*df*	Mean Squares	*F*-ratio	*P*
Habitat	0.09661	1	0.096608	4.9308	0.03531
Residuals	0.50941	26	0.019593		
Total	0.147551	27			

Table 5.4: Maximum effective stress observed in the two species tested, with varying Young's Modulus (E) values and applied forces (N).

Species	Force (N)	E (GPa)	Maximum Effective Stress (GPa)
Gyrinophilus porphyriticus	0.5	0.5	9.53
	0.5	1	8.89
	0.5	5	8.04
	0.5	10	7.91
	0.5	15	7.87
Eurycea wallacei	0.5	0.5	4.79
	0.5	1	4.45
	0.5	5	4.14
	0.5	10	4.09
	0.5	15	4.08
Eurycea wallacei	10	5	107
	10	15	91.3

CHAPTER 6: CONCLUSIONS

As hypothesized, aquatic and terrestrial species have different skull morphologies, as demonstrated by vomer (Chapter 1), mandible (Chapter 5), and cranium (Chapter 2) datasets. While cranium shape did not show classical convergence, secondarily aquatic species show similar shifts in morphospace relative to closely related terrestrial taxa. These shifts corresponded to changes in the jaw suspensory apparatus. Mandible morphology also depends on habitat, with aquatic species having relatively shorter and wider jaws than terrestrial species. Both findings support the hypothesis that feeding strategy strongly influences skull shape. Using the first Young's modulus values captured for an anamniote skull (Chapter 3), I performed a finite element analysis on two plethodontid jaws but found conflicting evidence for terrestrial species able to perform stronger bites. This suggests that suction feeding is the strongest selective force on the lower jaw (and perhaps, by extension, the whole skull), and that (contrary to implicit biases) the shift to land represents a relaxation of functional constraints rather than the imposition of new challenges.

REFERENCES

Anderson, J. S. (2012). Fossils, molecules, divergence times, and the origin of Salamandroidea. *Proceedings of the National Academy of Sciences*, 109(15), 5557-555

Anderson, P. S., Friedman, M., & Ruta, M. (2013). Late to the table: diversification of tetrapod mandibular biomechanics lagged behind the evolution of terrestriality. *Integrative & Comparative Biology*, 53(2).

Blankers, T., Adams, D. C., & Wiens, J. J. (2012). Ecological radiation with limited morphological diversification in salamanders. *Journal of evolutionary biology*, 25(4), 634-646.

Bonett, R. M., Steffen, M. A., Lambert, S. M., Wiens, J. J., & Chippindale, P. T. (2014). Evolution of paedomorphosis in plethodontid salamanders: ecological correlates and re-evolution of metamorphosis. *Evolution*, 68(2), 466-482.

Bookstein, F. L. (1997). Landmark methods for forms without landmarks: morphometrics of group differences in outline shape. *Medical image analysis*, 1(3), 225-243.

Capshaw, G., Soares, D., & Carr, C. E. (2019). Bony labyrinth morphometry reveals hidden diversity in lungless salamanders (Family Plethodontidae): Structural correlates of ecology, development, and vision in the inner ear. *Evolution*, *73*(10), 2135-2150.

Chippindale, P. T., Bonett, R. M., Baldwin, A. S., & Wiens, J. J. (2004). Phylogenetic evidence for a major reversal of life-history evolution in plethodontid salamanders. *Evolution*, 58(12), 2809-2822.

Currey, J. D. (1987). The evolution of the mechanical properties of amniote bone. *Journal of biomechanics*, 20(11-12), 1035-1044.

Currey, J. D. (1988). The effect of porosity and mineral content on the Young's modulus of elasticity of compact bone. *Journal of biomechanics*, 21(2), 131-139.

Currey, J. D. (2010). Mechanical properties and adaptations of some less familiar bony tissues. *Journal of the Mechanical Behavior of Biomedical Materials*, 3(5), 357-372.

Currey, J. D., Landete-Castillejos, T., Estevez, J. A., Olguin, A., Garcia, A. J., & Gallego, L. (2009). The Young's Modulus and impact energy absorption of wet and dry deer cortical bone. *The Open Bone Journal*, 1(1).

Cvijanović, M., Ivanović, A., Kalezić, M. L., & Zelditch, M. L. (2014). The ontogenetic origins of skull shape disparity in the *Triturus cristatus* group. *Evolution & Development*, 16(5), 306-317.

Cvijanović, M., Üzüm, N., Ivanović, A., Avci, A., Özcan, Ç. G., & Olgun, K. (2017). Variation in skull size and shape in a newt species with male-biased sexual dimorphism. *Herpetological Journal*, 27(1), 41-46

Darcy, H. E. (2015). Additional research and taxonomic resolution of salamanders (Amphibia: Caudata) from the Mio-Pliocene Gray Fossil Site, TN (Doctoral dissertation, East Tennessee State University).

Darda, D. M., & Wake, D. B. (2015). Osteological variation among extreme morphological forms in the Mexican salamander genus *Chiropterotriton* (Amphibia: Plethodontidae): Morphological evolution and homoplasy. *PloS one*, 10(6), e0127248.

Deban, S. M., & Richardson, J. C. (2017). A peculiar mechanism of bite-force enhancement in lungless salamanders revealed by a new geometric method for modeling muscle moments. *Journal of Experimental Biology*, *220*(19), 3588-3597.

Denoël, M., Ivanović, A., Džukić, G., & Kalezić, M. L. (2009). Sexual size dimorphism in the evolutionary context of facultative paedomorphosis: insights from European newts. *BMC Evolutionary Biology*, 9(1), 278.

Denoël, M., Joly, P., & Whiteman, H. H. (2005). Evolutionary ecology of facultative paedomorphosis in newts and salamanders. *Biological Reviews*, 80(4), 663-671.

Donnelly, E., Baker, S. P., Boskey, A. L., & van der Meulen, M. C. (2006). Effects of surface roughness and maximum load on the mechanical properties of cancellous bone measured by nanoindentation. *Journal of Biomedical Materials Research Part A: An Official Journal of The Society for Biomaterials, The Japanese Society for Biomaterials,* and *The Australian Society for Biomaterials* and *the Korean Society for Biomaterials*, 77(2), 426-435.

Duellman, W. and Sweet, S. (1999) 'Distribution patterns of amphibians in the neartic region of North America', in Duellman, W. (ed) *Patterns of Distribution of Amphibians, A Global Perspective*: The Johns Hopkins University Press.

Dumont, E. R., Grosse, I. R., & Slater, G. J. (2009). Requirements for comparing the performance of finite element models of biological structures. *Journal of Theoretical Biology*, 256(1), 96-103.

Ebenstein, D. M., & Pruitt, L. A. (2006). Nanoindentation of biological materials. *Nano today*, 1(3), 26-33.

Edgington, H. A., & Taylor, D. R. (2019). Ecological contributions to body shape evolution in salamanders of the genus *Eurycea* (Plethodontidae). *Plos one*, 14(5), e0216754.

Engineering ToolBox, (2003). Young's Modulus, Tensile Strength and Yield Strength Values for some Materials. [online] Available at: https://www.engineeringtoolbox.com/young-modulus-d_417.html [Accessed 18 April 2023].

Erickson, G. M. (1997). The evolution of the biomechanical attributes of long bones. University of California, Berkeley.

Ferrara, T. L., Boughton, P., Slavich, E., & Wroe, S. (2013). A novel method for single sample multi-axial nanoindentation of hydrated heterogeneous tissues based on testing great white shark jaws. *PloS one*, 8(11), e81196.

Fortuny, J., Marcé-Nogué, J., & Konietzko-Meier, D. (2017). Feeding biomechanics of Late Triassic metoposaurids (Amphibia: Temnospondyli): a 3D finite element analysis approach. *Journal of Anatomy*, 230(6), 752-765.

Fortuny, J., Marcé-Nogué, J., Heiss, E., Sanchez, M., Gil, L., & Galobart, À. (2015). 3D bite modeling and feeding mechanics of the largest living amphibian, the Chinese giant salamander *Andrias davidianus* (Amphibia: Urodela). *PLoS One*, 10(4), e0121885.

Fortuny, J., Marcé-Nogué, J., Steyer, J., de Esteban-Trivigno, S., Mujal, E., & Gil, L. (2016). Comparative 3D analyses and palaeoecology of giant early amphibians (Temnospondyli: Stereospondyli). *Scientific Reports*, 6(1), 1-10.

Frost, Darrel R. (2016). Amphibian Species of the World: an Online Reference. Version 6.0. American Museum of Natural History. *Retrieved 12 January 2017.*

Gil, L., Marcé-Nogué, J., & Sánchez, M. (2015). Insights into the controversy over materials data for the comparison of biomechanical performance in vertebrates. *Palaeontologia Electronica*, *18*(1), 1-24.

Gruntmejer, K., Konietzko-Meier, D., Marcé-Nogué, J., Bodzioch, A., & Fortuny, J. (2019). Cranial suture biomechanics in *Metoposaurus krasiejowensis* (Temnospondyli, Stereospondyli) from the upper Triassic of Poland. *Journal of Morphology*, 280(12), 1850-1864.

Hanken, J. (1984). Miniaturization and its effects on cranial morphology in plethodontid salamanders, genus *Thorius* (Amphibia: Plethodontidae). I. Osteological variation. *Biological Journal of the Linnean Society*, 23(1), 55-75.

Heiss, E., Natchev, N., Gumpenberger, M., Weissenbacher, A., & Van Wassenbergh, S. (2013). Biomechanics and hydrodynamics of prey capture in the Chinese giant salamander reveal a high-performance jaw-powered suction feeding mechanism. *Journal of the Royal Society Interface*, 10(82), 20121028.

Heiss, E., Natchev, N., Salaberger, D., Gumpenberger, M., Rabanser, A., & Weisgram, J. (2010). Hurt yourself to hurt your enemy: new insights on the function of the bizarre antipredator mechanism in the salamandrid *Pleurodeles waltl*. *Journal of Zoology*, 280(2), 156-162.

Heiss, E., Schwarz, D., & Konow, N. (2019). Chewing or not? Intraoral food processing in a salamandrid newt. *Journal of Experimental Biology*, 222(6), jeb189886.

Hime, P. M., Lemmon, A. R., Lemmon, E. C. M., Prendini, E., Brown, J. M., Thomson, R. C., ... & Weisrock, D. W. (2021). Phylogenomics reveals ancient gene tree discordance in the amphibian tree of life. *Systematic biology*, *70*(1), 49-66.

Housworth, E. A., Martins, E. P., & Lynch, M. (2004). The phylogenetic mixed model. *The American Naturalist*, *163*(1), 84-96.

Hudson, N. J., Bennett, M. B., & Franklin, C. E. (2004). Effect of aestivation on long bone mechanical properties in the green-striped burrowing frog, *Cyclorana alboguttata*. *Journal of experimental biology*, 207(3), 475-482.

Iordansky, N. N. (2005). Paedomorphosis, neoteny, and evolution. *Zoologicheskiĭ Zhurnal, 84*(10), 1176-1187.

Jablonski, D. (2000). Micro-and macroevolution: scale and hierarchy in evolutionary biology and paleobiology. *Paleobiology*, 15-52.

Jetz, W., & Pyron, R.A. (2018). The interplay of past diversification and evolutionary isolation with present imperilment across the amphibian tree of life. *Nat Ecol Evol* 2, 850–858 (2018).

Jia, J., Li, G., & Gao, K. Q. (2022). Palatal morphology predicts the paleobiology of early salamanders. *Elife*, *11*, e76864.

Konietzko-Meier, D., Gruntmejer, K., Marcé-Nogué, J., Bodzioch, A., & Fortuny, J. (2018). Merging cranial histology and 3D-computational biomechanics: a review of the feeding ecology of a Late Triassic temnospondyl amphibian. *PeerJ*, 6, e4426.

Kushch, V. I., Dub, S. N., & Litvin, P. M. (2007). Determination of the young modulus from elastic section of the Berkovich indenter loading curve. *Journal of Superhard Materials*, 29, 228-234.

Larsen Jr., J. H., & Guthrie, D. J. (1975). The feeding system of terrestrial tiger salamanders (*Ambystoma tigrinum melanostictum* Baird). *Journal of Morphology*, 147(2), 137-153.

Lauder, G. V., & Reilly, S. M. (1990). Metamorphosis of the feeding mechanism in tiger salamanders (*Ambystoma tigrinum*): the ontogeny of cranial muscle mass. *Journal of Zoology*, *222*(1), 59-74.

Lauder, G. V., & Reilly, S. M. (1996). The mechanistic bases of behavioral evolution: a multivariate analysis of musculoskeletal function. *Phylogenies and the Comparative Method in Animal Behavior*, 104-137.

Lauder, G.V. (1996). The argument from design. In M.R. Rose and G.V. Lauder (Eds.) *Adaption* (pp. 511). San Diego, California: Academic Press, Inc.

Levis, N. A., & Pfennig, D. W. (2018, March). Phenotypic plasticity, canalization, and the origins of novelty: evidence and mechanisms from amphibians. In *Seminars in cell & developmental biology*. Academic Press.

Lombard, R. E., & Wake, D. B. (1976). Tongue evolution in the lungless salamanders, family Plethodontidae I. Introduction, theory and a general model of dynamics. *Journal of Morphology*, 148(3), 265-286.

Lynch, M. (1991). Methods for the analysis of comparative data in evolutionary biology. *Evolution*, *45*(5), 1065-1080.

Lynch, M. (2007). The frailty of adaptive hypotheses for the origins of organismal complexity. *Proceedings of the National Academy of Sciences*, *104*(suppl 1), 8597-8604.

Marks, S. B. (2000). *The biology of plethodontid salamanders*. Springer, Boston, MA.

Miller, B. T., & Larsen Jr, J. H. (1990). Comparative kinematics of terrestrial prey capture in salamanders and newts (Amphibia: Urodela: Salamandridae). *Journal of Experimental Zoology*, 256(2), 135-153.

Moazen, M., Curtis, N., Evans, S. E., O'Higgins, P., & Fagan, M. J. (2008). Combined finite element and multibody dynamics analysis of biting in a *Uromastyx hardwickii* lizard skull. *Journal of Anatomy*, 213(5), 499-508.

Moazen, M., Curtis, N., O'Higgins, P., Evans, S. E., & Fagan, M. J. (2009). Biomechanical assessment of evolutionary changes in the lepidosaurian skull. *Proceedings of the National Academy of Sciences*, 106(20), 8273-8277.

Nye, H. L., Cameron, J. A., Chernoff, E. A., & Stocum, D. L. (2003). Extending the table of stages of normal development of the axolotl: limb development. *Developmental dynamics: an official publication of the American Association of Anatomists*, 226(3), 555-560.

Oliver, W. C., & Pharr, G. M. (2004). Measurement of hardness and elastic modulus by instrumented indentation: Advances in understanding and refinements to methodology. *Journal of materials research*, 19(1), 3-20.

Oyen, M. (2013). Nanoindentation of biological and biomimetic materials. *Experimental Techniques*, 37(1), 73-87.

Panagiotopoulou, O. (2009). Finite element analysis (FEA): applying an engineering method to functional morphology in anthropology and human biology. *Annals of human biology*, 36(5), 609-623.

Parra-Olea, G., & Wake, D. B. (2001). Extreme morphological and ecological homoplasy in tropical salamanders. *Proceedings of the National Academy of Sciences*, 98(14), 7888-7891.

Pérez-Ben, C. M., Schoch, R. R., & Báez, A. M. (2018). Miniaturization and morphological evolution in Paleozoic relatives of living amphibians: a quantitative approach. *Paleobiology*, 44(1), 58-75.

Pipan T., & Culver D.C.(2012). Convergence and divergence in the subterranean realm: a reassessment. *Biol J Linnean Soc*. 2012;107(1):1–14.

Polly, P. D., Stayton, C. T., Dumont, E. R., Pierce, S. E., Rayfield, E. J., & Angielczyk, K. D. (2016). Combining geometric morphometrics and finite element analysis with evolutionary modeling: towards a synthesis. *Journal of Vertebrate Paleontology*, 36(4), e1111225.

Rayfield, E. J. (2007). Finite element analysis and understanding the biomechanics and evolution of living and fossil organisms. *Annu. Rev. Earth Planet. Sci.*, 35, 541-576.

Revell LJ (2012). phytools: An R package for phylogenetic comparative biology (and other things).”Methods in Ecology and Evolution, 3, 217-223.

Rohlf, F. (2013a). tpsDIG2, version 2.17. Department of Ecology and Evolution, State University of New York at Stony Brook.

Rohlf, F. (2013b). tpsUtil, version 1.58. Department of Ecology and Evolution, State University of New York at Stony Brook.

Rohlf, F. J., & Slice, D. (1990). Extensions of the Procrustes method for the optimal superimposition of landmarks. Systematic biology, 39(1), 40-59.

Rose, C. S., Heatwole, H., & Davies, M. (2003). The developmental morphology of salamander skulls. *Amphibian biology*, *5*, 1684-1781.

Ross, C. F., & Metzger, K. A. (2004). Bone strain gradients and optimization in vertebrate skulls. *Annals of Anatomy-Anatomischer Anzeiger*, 186(5-6), 387-396.

Rull, M., Solomon, J., & Konow, N. (2020). Elastic recoil action amplifies jaw closing speed in an aquatic feeding salamander. *Proceedings of the Royal Society B*, 287(1927), 20200428.

Santana, S. E., Grosse, I. R., & Dumont, E. R. (2012). Dietary hardness, loading behavior, and the evolution of skull form in bats. *Evolution: International Journal of Organic Evolution*, 66(8), 2587-2598.

Schlager S (2017). Morpho and Rvcg – Shape Analysis in R. In Zheng G, Li S, Szekely G (eds.), *Statistical Shape and Deformation Analysis*, 217–256. Academic Press. ISBN 9780128104934.

Schoch, R. R. (2014). Amphibian skull evolution: the developmental and functional context of simplification, bone loss and heterotopy. *Journal of Experimental Zoology Part B: Molecular and Developmental Evolution*, 322(8), 619-630.

Schwarz, D., Fedler, M. T., Lukas, P., & Kupfer, A. (2021). Form and function of the feeding apparatus of sirenid salamanders (Caudata: Sirenidae): Three-dimensional chewing and herbivory?. *Zoologischer Anzeiger*, 295, 99-116.

Schwarz, D., Konow, N., Roba, Y. T., & Heiss, E. (2020). A salamander that chews using complex, three-dimensional mandible movements. *Journal of Experimental Biology*, 223(5), jeb220749.

Schwenk, K. and Schwenk, K. (2000). An introduction to tetrapod feeding. In *Feeding* (ed. K. Schwenk), pp. 21-61. Elsevier.

Shaffer, H. B. (1984). Evolution in a paedomorphic lineage. II. Allometry and form in the Mexican ambystomatid salamanders. *Evolution, 38*(6), 1207-1218.

Shahar, R., Zaslansky, P., Barak, M., Friesem, A. A., Currey, J. D., & Weiner, S. (2007). Anisotropic Poisson's ratio and compression modulus of cortical bone determined by speckle interferometry. *Journal of biomechanics*, 40(2), 252-264.

Soares, D., & Niemiller, M. L. (2020). Extreme adaptation in caves. *The Anatomical Record*, 303(1), 15-23.

Stayton, C. T. (2006). Testing hypotheses of convergence with multivariate data: morphological and functional convergence among herbivorous lizards. *Evolution*, *60*(4), 824-841.

Stayton, C. T. (2011). Biomechanics on the half shell: functional performance influences patterns of morphological variation in the emydid turtle carapace. *Zoology*, 114(4), 213-223.

Strait, D. S., Wang, Q., Dechow, P. C., Ross, C. F., Richmond, B. G., Spencer, M. A., & Patel, B. A. (2005). Modeling elastic properties in finite-element analysis: how much precision is needed to produce an accurate model?. *The Anatomical Record Part A: Discoveries in Molecular, Cellular, and Evolutionary Biology: An Official Publication of the American Association of Anatomists*, 283(2), 275-287.

Üzüm, N., Ivanović, A., Gümüş, Ç., Avcı, A., & Olgun, K. (2015). Divergence in size, but not in shape: variation in skull size and shape within *Ommatotriton* newts. *Acta Zoologica*, 96(4), 478-486.

Vieites, D. R., Román, S. N., Wake, M. H., & Wake, D. B. (2011). A multigenic perspective on phylogenetic relationships in the largest family of salamanders, the Plethodontidae. *Molecular Phylogenetics and Evolution*, 59(3), 623-635.

Wainwright, P. C., Lauder, G. V., Osenberg, C. W., & Mittelbach, G. G. (1991). The functional basis of intraspecific trophic diversification in sunfishes. *The Unity of Evolutionary Biology*, 515-528.

Wake, D. B. (1966). Comparative Osteology and Evolution of the Lungless Salamanders, Family Plethodontidae. *Mem. South. Calif. Acad. Sci*. 4:130 pp.

Wake, D. B., Blackburn, D. C., & Lombard, R. E. (2015). Rampant homoplasy in complex characters: Repetitive convergent evolution of amphibian feeding structures. *Great transformations in vertebrate evolution*, 395-405.

Wake, D.B. & Deban, S.M. (2000). Terrestrial feeding in salamanders. In: Schwenk K, editor. *Feeding: Form, Function, Phylogeny*. San Diego: Academic Press. pp 95–116.

Wake, D. B., & Hanken, J. A. M. E. S. (2004). Direct development in the lungless salamanders: what are the consequences for developmental biology, evolution and phylogenesis?. *International Journal of Developmental Biology*, 40(4), 859-869.

Walmsley, C. W., McCurry, M. R., Clausen, P. D., & McHenry, C. R. (2013). Beware the black box: investigating the sensitivity of FEA simulations to modelling factors in comparative biomechanics. *PeerJ*, *1*, e204.

Whiteman, H. H. (1994). Evolution of facultative paedomorphosis in salamanders. *The Quarterly review of biology*, 69(2), 205-221.

Wilbur, H. M., & Collins, J. P. (1973). Ecological Aspects of Amphibian Metamorphosis: Nonnormal distributions of competitive ability reflect selection for facultative metamorphosis. *Science*, 182(4119), 1305-1314.

Wilder, I. W. (1925). *The morphology of amphibian metamorphosis* (Vol. 6). Smith College.

Wray, K. P., & Steppan, S. J. (2017). Ecological opportunity, historical biogeography and diversification in a major lineage of salamanders. *Journal of Biogeography*, 44(4), 797-809.

Zhang, P., Chen, Y. Q., Zhou, H., Liu, Y. F., Wang, X. L., Papenfuss, T. J., ... & Qu, L. H. (2006). Phylogeny, evolution, and biogeography of Asiatic Salamanders (Hynobiidae). *Proceedings of the National Academy of Sciences*, 103(19), 7360-7365.

Zhou, Z., Fortuny, J., Marcé-Nogué, J., & Skutschas, P. P. (2017). Cranial biomechanics in basal urodeles: the Siberian salamander (*Salamandrella keyserlingii*) and its evolutionary and developmental implications. *Scientific reports*, 7(1), 1-11.

Zysset, P. K., Guo, X. E., Hoffler, C. E., Moore, K. E., & Goldstein, S. A. (1999). Elastic modulus and hardness of cortical and trabecular bone lamellae measured by nanoindentation in the human femur. *Journal of biomechanics*, 32(10), 1005-1012.

APPENDIX A: SPECIMEN DATA SOURCES FOR CHAPTER 2

Table A.1. The list of specimens used for Chapter 2 to analyze the vomer morphology of Spelerpini salamanders. Image Source indicates if the data is two- or three-dimensional, the source of the data is given, and the permanent repository of the specimen is listed.

Catalogue Number	Species	Image Source	Scan Data Source	Specimen Repository
BMNH 1957.1.7.86	*Eurycea lucifuga*	microCT scan	www.phenome10k.org	Natural History Museum, London, UK
BMNH 1957.1.8.37-37	*Pseudotriton montanus*	microCT scan	www.phenome10k.org	Natural History Museum, London, UK
BMNH 1957.1.8.39	*Sterochilus marginatus*	microCT scan	www.phenome10k.org	Natural History Museum, London, UK
BMNH 1957.1.8.41	*Eurycea spelaea*	microCT scan	www.phenome10k.org	Natural History Museum, London, UK
DCP 4510	*Eurycea cirrigera*	Photographed by H. Darcy	-	Dennis C. Parmley personal collection, East Tennessee State University Vertebrate Paleontology Laboratory, Johnson City, TN, USA
ETVP "LBL"	*Eurycea lucifuga*	microCT scan	Scanned by H. Darcy	East Tennessee State University Vertebrate Paleontology Laboratory, Johnson City, TN, USA
ETVP 2905	*Stereochilus marginatus*	Photographed by H. Darcy	-	East Tennessee State University Vertebrate Paleontology Laboratory, Johnson City, TN, USA
FMNH 109962	*Haideotriton wallacei*	microCT scan	Scanned by H. Darcy	Field Museum of Natural History, Chicago, IL, USA
FMNH 167146	*Sterochilus marginatus*	microCT scan	Scanned by H. Darcy	Field Museum of Natural History, Chicago, IL, USA
FMNH 5107	*Eurycea neotenes*	microCT scan	Scanned by H. Darcy	Field Museum of Natural History, Chicago, IL, USA
FMNH 55090	*Eurycea neotenes*	microCT scan	Scanned by H. Darcy	Field Museum of Natural History, Chicago, IL, USA
FMNH 55101	*Eurycea neotenes*	microCT scan	Scanned by H. Darcy	Field Museum of Natural History, Chicago, IL, USA
FMNH 5843	*Eurycea quadridigitata*	microCT scan	Scanned by H. Darcy	Field Museum of Natural History, Chicago, IL, USA
FMNH 91041	*Eurycea latitans*	microCT scan	Scanned by H. Darcy	Field Museum of Natural History, Chicago, IL, USA
FMNH 91385	*Eurycea quadridigitata*	microCT scan	Scanned by H. Darcy	Field Museum of Natural History, Chicago, IL, USA
FMNH 91386	*Eurycea quadridigitata*	microCT scan	Scanned by H. Darcy	Field Museum of Natural History, Chicago, IL, USA
FMNH 91388	*Eurycea quadridigitata*	microCT scan	Scanned by H. Darcy	Field Museum of Natural History, Chicago, IL, USA
FMNH 93404	*Eurycea latitans*	microCT scan	Scanned by H. Darcy	Field Museum of Natural History, Chicago, IL, USA
FMNH55104	*Eurycea neotenes*	microCT scan	Scanned by H. Darcy	Field Museum of Natural History, Chicago, IL, USA

Table A.1 continued. The list of specimens used for Chapter 2 to analyze the vomer morphology of Spelerpini salamanders. Image Source indicates if the data is two- or three-dimensional, the source of the data is given, and the permanent repository of the specimen is listed.

Catalogue Number	Species	Image Source	Scan Data Source	Specimen Repository
MNHN 1961_423	*Pseudotriton ruber*	microCT scan	www.phenome10k.org	Muséum national d'Histoire naturelle, Paris, France
MNHN 2007-2498	*Eurycea bislineata*	microCT scan	www.phenome10k.org	Muséum national d'Histoire naturelle, Paris, France
NCSM 82390	*Gyrinophilus porphyriticus*	Photographed by H. Darcy	-	East Tennessee State University Vertebrate Paleontology Laboratory, Johnson City, TN, USA
NCSM 82393	*Pseudotriton ruber*	Photographed by H. Darcy	-	North Carolina Museum of Natural History
TNHC 50916	*Eurycea sosorum*	microCT scan	www.phenome10k.org	Texas Memorial Museum, Texas Natural History Collections, Austin, Texas, USA
TNHC 60202	*Eurycea waterlooensis*	microCT scan	www.phenome10k.org	Texas Memorial Museum, Texas Natural History Collections, Austin, Texas, USA
ZMB 13190	*Eurycea longicauda*	microCT scan	www.phenome10k.org	Zoological Museum of Berlin, Berlin, Germany
ZMB 29766	*Gyrinophilus porphyriticus*	microCT scan	www.phenome10k.org	Zoological Museum of Berlin, Berlin, Germany

APPENDIX B: SPECIMEN DATA SOURCES FOR CHAPTER 3

Table B.1. The list of specimens used for Chapter 3 to analyze the three-dimensional morphology of crania in Spelerpini and *Ambystoma* salamanders. The source of the data and the permanent repository of the specimen are listed.

Catalogue Number	**Species**	**Scan Data Source**	**Specimen Repository**
"1"	*Gyrinophilus porphyriticus*	Scanned by H. Darcy	Teaching collection, School of Integrative Biology, University of Illinois Urbana-Champaign, Urbana, IL, USA
"823"	*Eurycea cirrigera*	Scanned by H. Darcy	Teaching collection, School of Integrative Biology, University of Illinois Urbana-Champaign, Urbana, IL, USA
BMNH 1914.1.28.247-248	*Ambystoma dumerilii*	www.phenome10k.org	Natural History Museum, London, UK
BMNH 1957.1.7.84-85	*Eurycea cirrigera*	www.phenome10k.org	Natural History Museum, London, UK
BMNH 1957.1.7.86	*Eurycea lucifuga*	www.phenome10k.org	Natural History Museum, London, UK
BMNH 1957.1.7.86	*Eurycea lucifuga*	www.phenome10k.org	Natural History Museum, London, UK
BMNH 1957.1.7.88-89	*Eurycea neotenes*	www.phenome10k.org	Natural History Museum, London, UK
BMNH 1957.1.8.37-38	*Pseudotriton montanus*	www.phenome10k.org	Natural History Museum, London, UK
BMNH 1957.1.8.39	*Stereochilus marginatus*	www.phenome10k.org	Natural History Museum, London, UK
BMNH 1957.1.8.41	*Eurycea spelaea*	www.phenome10k.org	Natural History Museum, London, UK
FMNH 11937	*Ambystoma tigrinum mavortium*	Scanned by H. Darcy	Field Museum of Natural History, Chicago, IL, USA
FMNH 167146	*Stereochilus marginatus*	Scanned by H. Darcy	Field Museum of Natural History, Chicago, IL, USA
FMNH 18070	*Ambystoma tigrinum mavortium*	Scanned by H. Darcy	Field Museum of Natural History, Chicago, IL, USA
FMNH 18074	*Ambystoma tigrinum mavortium*	Scanned by H. Darcy	Field Museum of Natural History, Chicago, IL, USA
FMNH 228432	*Ambystoma andersoni*	Scanned by H. Darcy	Field Museum of Natural History, Chicago, IL, USA
FMNH 228434	*Ambystoma andersoni*	Scanned by H. Darcy	Field Museum of Natural History, Chicago, IL, USA
FMNH 228440	*Ambystoma silvense*	Scanned by H. Darcy	Field Museum of Natural History, Chicago, IL, USA
FMNH 228444	*Ambystoma silvense*	Scanned by H. Darcy	Field Museum of Natural History, Chicago, IL, USA

Table B.1. continued. The list of specimens used for Chapter 3 to analyze the three-dimensional morphology of crania in Spelerpini and *Ambystoma* salamanders. The source of the data and the permanent repository of the specimen are listed.

Catalogue Number	Species	Scan Data Source	Specimen Repository
FMNH 228447	*Ambystoma silvense*	Scanned by H. Darcy	Field Museum of Natural History, Chicago, IL, USA
FMNH 37421	*Ambystoma tigrinum mavortium*	Scanned by H. Darcy	Field Museum of Natural History, Chicago, IL, USA
FMNH 55090	*Eurycea neotenes*	Scanned by H. Darcy	Field Museum of Natural History, Chicago, IL, USA
FMNH 55101	*Eurycea neotenes*	Scanned by H. Darcy	Field Museum of Natural History, Chicago, IL, USA
FMNH 55104	*Eurycea neotenes*	Scanned by H. Darcy	Field Museum of Natural History, Chicago, IL, USA
FMNH 55107	*Eurycea neotenes*	Scanned by H. Darcy	Field Museum of Natural History, Chicago, IL, USA
FMNH 84685	*Ambystoma tigrinum mavortium*	Scanned by H. Darcy	Field Museum of Natural History, Chicago, IL, USA
FMNH 93403	*Eurycea latitans*	Scanned by H. Darcy	Field Museum of Natural History, Chicago, IL, USA
INHS 14224	*Ambystoma lermaensis*	Scanned by H. Darcy	Illinois Natural History Survey, University of Illinois Urbana-Champaign, Champaign, IL, USA
INHS 14227	*Ambystoma lermaensis*	Scanned by H. Darcy	Illinois Natural History Survey, University of Illinois Urbana-Champaign, Champaign, IL, USA
INHS 25043	*Ambystoma bombypellum*	Scanned by H. Darcy	Illinois Natural History Survey, University of Illinois Urbana-Champaign, Champaign, IL, USA
INHS 28108	*Ambystoma altamirani*	Scanned by H. Darcy	Illinois Natural History Survey, University of Illinois Urbana-Champaign, Champaign, IL, USA
INHS 28125	*Ambystoma gracile*	Scanned by H. Darcy	Illinois Natural History Survey, University of Illinois Urbana-Champaign, Champaign, IL, USA
INHS 28178	*Ambystoma altamirani*	Scanned by H. Darcy	Illinois Natural History Survey, University of Illinois Urbana-Champaign, Champaign, IL, USA
INHS 28546	*Ambystoma leorae*	Scanned by H. Darcy	Illinois Natural History Survey, University of Illinois Urbana-Champaign, Champaign, IL, USA
INHS 29165	*Ambystoma ordinarium*	Scanned by H. Darcy	Illinois Natural History Survey, University of Illinois Urbana-Champaign, Champaign, IL, USA
INHS 30888	*Ambystoma rivulare*	Scanned by H. Darcy	Illinois Natural History Survey, University of Illinois Urbana-Champaign, Champaign, IL, USA
INHS 35314	*Ambystoma amblycephalum*	Scanned by H. Darcy	Illinois Natural History Survey, University of Illinois Urbana-Champaign, Champaign, IL, USA
INHS 53581	*Ambystoma rosaceum*	Scanned by H. Darcy	Illinois Natural History Survey, University of Illinois Urbana-Champaign, Champaign, IL, USA

Table B.1. continued. The list of specimens used for Chapter 3 to analyze the three-dimensional morphology of crania in Spelerpini and *Ambystoma* salamanders. The source of the data and the permanent repository of the specimen are listed.

Catalogue Number	Species	Scan Data Source	Specimen Repository
MNHN 1961 462	*Pseudotriton ruber*	www.phenome10k.org	Muséum national d'Histoire naturelle, Paris, France
MNHN 2007-2498	*Eurycea bislineata*	www.phenome10k.org	Muséum national d'Histoire naturelle, Paris, France
MVZ 63775	*Ambystoma gracile*	www.phenome10k.org	Museum of Vertebrate Zoology, University of California, Berkeley, California, U.S.A.
TNHC 17991	*Ambystoma tigrinum*	www.phenome10k.org	Texas Memorial Museum, Texas Natural History Collections, Austin, Texas, USA
TNHC 20255	*Eurycea robusta*	www.phenome10k.org	Texas Memorial Museum, Texas Natural History Collections, Austin, Texas, USA
TNHC 50916	*Eurycea sosorum*	www.phenome10k.org	Texas Memorial Museum, Texas Natural History Collections, Austin, Texas, USA
TNHC 60202	*Eurycea waterlooensis*	www.phenome10k.org	Texas Memorial Museum, Texas Natural History Collections, Austin, Texas, USA
UF 26607	*Ambystoma maculatum*	www.phenome10k.org	Florida Museum of Natural History, University of Florida, Gainesville, Florida, U.S.A
UIUC 155	*Eurycea cirrigera*	Scanned by H. Darcy	Teaching collection, School of Integrative Biology, University of Illinois Urbana-Champaign, Urbana, IL, USA
ZMB 13190	*Eurycea longicauda*	www.phenome10k.org	Zoological Museum of Berlin, Berlin, Germany
ZMB 84351	*Ambystoma mexicanum*	www.phenome10k.org	Zoological Museum of Berlin, Berlin, Germany